

Uplift history of the Sila Massif, southern Italy, deciphered from cosmogenic ^{10}Be erosion rates and river longitudinal profile analysis

Valerio Olivetti,¹ Andrew J. Cyr,² Paola Molin,¹ Claudio Faccenna,¹ and Darryl E. Granger³

Received 7 October 2011; revised 20 February 2012; accepted 27 March 2012; published 17 May 2012.

[1] The Sila Massif in the Calabrian Arc (southern Italy) is a key site to study the response of a landscape to rock uplift. Here an uplift rate of ~ 1 mm/yr has imparted a deep imprint on the Sila landscape recorded by a high-standing low-relief surface on top of the massif, deeply incised fluvial valleys along its flanks, and flights of marine terraces in the coastal belt. In this framework, we combined river longitudinal profile analysis with hillslope erosion rates calculated by ^{10}Be content in modern fluvial sediments to reconstruct the long-term uplift history of the massif. Cosmogenic data show a large variation in erosion rates, marking two main domains. The samples collected in the high-standing low-relief surface atop Sila provide low erosion rates (from 0.09 ± 0.01 to 0.13 ± 0.01 mm/yr). Conversely, high values of erosion rate (up to 0.92 ± 0.08 mm/yr) characterize the incised fluvial valleys on the massif flanks. The analyzed river profiles exhibit a wide range of shapes diverging from the commonly accepted equilibrium concave-up form. Generally, the studied river profiles show two or, more frequently, three concave-up segments bounded by knickpoints and characterized by different values of concavity and steepness indices. The wide variation in cosmogenic erosion rates and the non-equilibrated river profiles indicate that the Sila landscape is in a transient state of disequilibrium in response to a strong and unsteady uplift not yet counterbalanced by erosion.

Citation: Olivetti, V., A. J. Cyr, P. Molin, C. Faccenna, and D. E. Granger (2012), Uplift history of the Sila Massif, southern Italy, deciphered from cosmogenic ^{10}Be erosion rates and river longitudinal profile analysis, *Tectonics*, 31, TC3007, doi:10.1029/2011TC003037.

1. Introduction

[2] Convergent margins are ideal sites to recognize the evolution of Earth's topography as a result of interacting tectonics, climate and erosion. The presence of a mountain chain suggests a dominance of tectonics in building topography until erosion compensates uplift. This tendency of geomorphic systems to counterbalance tectonic input could generate a negative feedback. Indeed, as a low-relief landscape is uplifted by tectonics, erosion rates increase over time in response to channel and hillslope steepening, enhanced by orographic precipitation [Whipple, 2001]. This increase in erosion rate tends to decrease excess elevation produced by tectonics [Ahnert, 1970] and simultaneously leads isostatic exhumation and an increase in the mean elevation [Molnar

and England, 1990; Burbank, 2002; Champagnac *et al.*, 2007]. Regardless, if climatic, tectonic and lithologic conditions are constant, a dynamic equilibrium between uplift and erosion is established, generating a steady state landscape [Hack, 1960; Willett and Brandon, 2002]. If the time scale of tectonic perturbation is sufficiently long compared with landscape response time (0.25–2.5 Ma), then tectonic forcing could be considered constant [e.g., Schumm and Lichty, 1965]. Conversely, climatic perturbation, especially during the Quaternary, may be too rapid to allow for steady state conditions [Whipple, 2001]. In an actively uplifting chain the landscape may be in a transient state of disequilibrium in response to climatic and tectonic inputs. Although hydrography occupies a small percentage of land surface it plays an important role in landscape evolution because it transmits tectonic and climatic signals throughout the landscape and dictates the slope processes that denude the land surface [Whipple and Tucker, 1999]. This sensitivity of river systems to climatic, and particularly to tectonic, perturbation makes the fluvial network a potential source of information about tectonic forcing on a landscape. At the catchment scale, evidence of the landscape response to climatic, and particularly tectonic, perturbation is present in the shape of stream longitudinal profiles [e.g., Wobus *et al.*, 2006, and references therein]. In this respect, bedrock channels are good targets for

¹Dipartimento Scienze Geologiche, Università Roma TRE, Rome, Italy.

²U.S. Geological Survey, Menlo Park, California, USA.

³Department of Earth and Atmospheric Sciences, Purdue University, West Lafayette, Indiana, USA.

Corresponding author: V. Olivetti, Dipartimento Scienze Geologiche, Università Roma TRE, Largo S. Leonardo Murialdo 1, I-00146 Rome, Italy. (volivetti@uniroma3.it)

Copyright 2012 by the American Geophysical Union.
0278-7407/12/2011TC003037

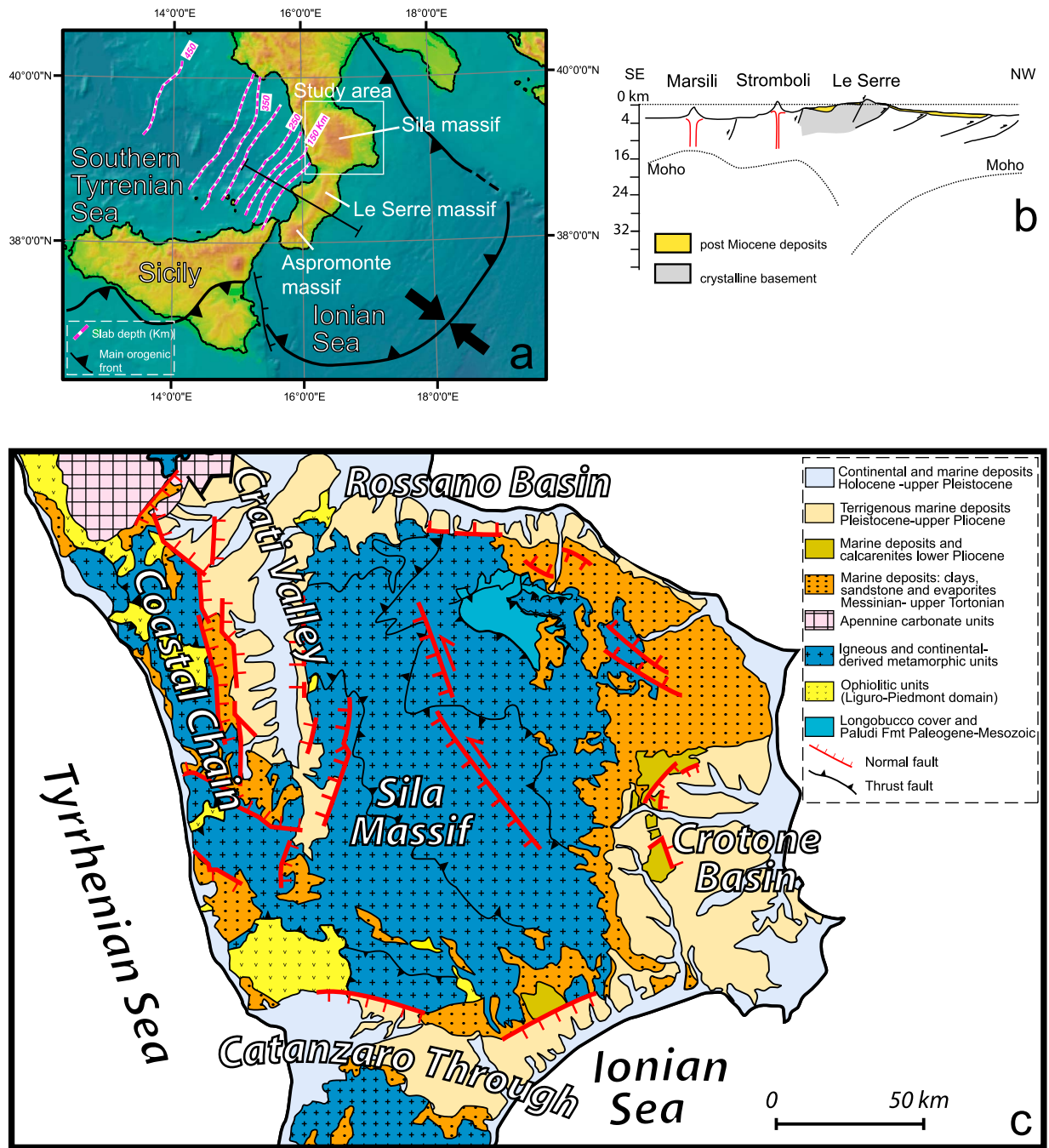


Figure 1. (a) Topography, bathymetry and main tectonic features of southern Italy (square: study area). Purple dashed lines are depth contour lines of the Wadati-Benioff zone associated with the Calabria subduction zone. (b) Crustal thickness along a NW-SE profile (indicated in Figure 1a) across central Calabria. Crustal thickness is from receiver function [Piana Agostinetti and Amato, 2009] and seismic [Suhadolc and Panza, 1989] data. (c) Geologic map of the Sila Massif.

longitudinal profile analysis because they provide the primary mechanism of incision in non-glaciated tectonically active areas [Hancock et al., 1998] and are the best expression of the feedback between tectonics and erosion, registering changes in base level (tectonic or eustatic) by variations in channel slope.

[3] One example of a transient landscape characterized by bedrock channels is the Sila Massif in the Calabrian Arc (southern Italy). The Calabrian Arc is an orogenic wedge

seated on top of a narrow subduction zone (Figure 1a). Here the uplift/erosion process likely started at a slow rate in the late Tertiary and underwent a strong acceleration in the middle Pleistocene [Westaway, 1993; Tortorici et al., 2003; Molin et al., 2004, and references therein]. Indeed, apatite and zircon fission track and Ar-Ar radiometric data show a major exhumation phase from 25 to 15 Ma [Thomson, 1994; Rossetti et al., 2001]. Pliocene alluvial deposits record that at least part of the Sila and the surrounding ridges (Catena

Costiera, and Le Serre) were already emerged and shaped by surface processes [Colella, 1995; Cavazza and DeCelles, 1998]. Relicts of the landscapes that served as a source of these alluvial deposits are probably represented by the low-relief surfaces located on top of the main Calabrian mountains [Ghisetti, 1981; Sorriso-Valvo and Sylvester, 1993; Molin et al., 2004]. These surfaces developed during stable or slowly lowering base level conditions [Molin et al., 2004, and references therein]. During the Quaternary, the Calabrian Arc was affected by a strong regional uplift, characterized by high uplift rates (~ 1 mm/yr) and locally enhanced by extensional tectonics [e.g., Dumas et al., 1987; Cucci and Cinti, 1998; Tortorici et al., 2003; Molin et al., 2004; Zecchin et al., 2004; Robustelli et al., 2009]. However, only during the last 200–400 kyr uplift rates are relatively well constrained by paleontological and radiometric dating [Ogniben, 1973; Barrier et al., 1986; Miyauchi et al., 1994; Balescu et al., 1997; Pirazzoli et al., 1997; Antonioli et al., 2006; Ferranti et al., 2009], whereas the time and rate of uplift during its early stages remain poorly constrained.

[4] In this study we coupled the analysis of the longitudinal profiles of streams draining the Sila Massif with erosion rates calculated from the ^{10}Be concentrations in modern fluvial sediments. The concentration of cosmogenic ^{10}Be isotopes reflects the averaged erosion rate of a drainage basin measured over the time required to erode cosmic ray penetration length, i.e., ~ 60 cm of rock of density of 2.6 g/cm^3 [Masarik and Reedy, 1995]. This time depends exactly on the erosion rate itself and vary from 600 yr for high erosion rates (i.e., 1 mm/yr) to 6 ka for low erosion rate of 0.1 mm/yr. The main goal of this paper is to compare new bedrock channel morphology and late Pleistocene–Present erosion rates to existing uplift rates from thermochronology and radiometric dating of marine terraces to investigate the history of Sila Massif upheaval in the context of the tectonic and geodynamic evolution of the Calabrian Arc.

2. Geologic Setting

[5] The Calabrian Arc zone in the Central Mediterranean constitutes the forearc belt of the active subduction of the Ionian basin. The Wadati-Benioff zone extends for only 200 km, dipping toward the northwest at about 70° down to ~ 500 km depth (Figure 1a) [Selvaggi and Chiarabba, 1995; Chiarabba et al., 2008]. The history of the Calabrian subduction zone is related to the southwestward retrograde motion of the trench, leading first to the backarc extension of the Liguro-Provençal basin and then of the Tyrrhenian basins [Malinverno and Ryan, 1986; Patacca et al., 1990; Royden, 1993; Rosenbaum and Lister, 2004; Casero and Roue, 1994; Faccenna et al., 2004]. Pulses of oceanic spreading in the Tyrrhenian formed the Vavilov basin (4–5 Ma) and then the Marsili Basin (2.1–1.6 Ma) [Kastens et al., 1988; Sartori et al., 1989; Nicolosi et al., 2006] during 15° – 25° clockwise rotation of the Calabrian belt [Speranza et al., 2000; Mattei et al., 2007; Cifelli et al., 2007a]. The last pulse of Marsili basin spreading has been related to a re-organization of the plate system, reducing the width of the subduction zone to its present-day narrow configuration [Goes et al., 2004; Giardini and Velonà, 1991; Faccenna et al., 2005; Billi et al., 2007; Chiarabba et al., 2008]. Geodetic data show that spreading of the

Tyrrhenian basin is no longer active [D'Agostino and Selvaggi, 2004], however, arc perpendicular extension is active within Calabria and is accommodated by a system of N-S trending normal faults [Cello et al., 1982; Tortorici et al., 1995; Monaco and Tortorici, 2000; Galli and Scionti, 2006]. The onset of the regional uplift of the Calabria arc probably occurred at that time, between early and middle Pleistocene [Colella et al., 1987; Dramis, 1992; Miyauchi et al., 1994; Westaway, 1993; Ferranti et al., 2006], during the narrowing and deformation of the subduction system [Westaway, 1993; Gvirtzman and Nur, 1999; Faccenna et al., 2011].

[6] A wealth of marine terraces are spectacularly sculpted on the flank of the Calabria massif, making Calabria a key site in the Mediterranean for analysis of coastal sea level change [Gliozzi, 1987; Cosentino and Gliozzi, 1988; Westaway, 1993; Miyauchi et al., 1994; Cucci and Cinti, 1998; Amato and Cinque, 1999; Molin et al., 2002; Carobene, 2003; Zecchin et al., 2004; Ferranti et al., 2006; Robustelli et al., 2009]. In particular, the most widely represented and well preserved terraces order along the entire Calabrian coastline [Westaway, 1993; Ferranti et al., 2006; Antonioli et al., 2006] is associated to Marine Isotope Stage (MIS) 5.5, 132 ± 16 ka in age [Stirling et al., 1995], giving an uplift rate of c. 1 mm/yr. This value is confirmed by the littoral deposits dated to Isotope Stage 31–35, 1000–1200 ka, associated to highest terrace on top of the Aspromonte and Le Serre at an elevation of about 1050 m a.s.l. [Barrier et al., 1986; Miyauchi et al., 1994; Balescu et al., 1997]. Therefore, although some authors proposed a pulsing uplift [Miyauchi et al., 1994], the average estimate of the uplift rate over the last million year seems to be remained constant, suggesting a long-lasting evolution for the same geodynamic process.

[7] Despite several studies devoted to understanding the rate and distribution of costal uplift, disagreement still exists about its cause, and very few data are available on the early stage of uplift. The origin of the uplift has been ascribed to mechanisms as variable as slab break off [Westaway, 1993; Wortel and Spakman, 2000; Buiter et al., 2002], inflow of asthenospheric material [Gvirtzman and Nur, 1999; Doglioni et al., 2007], and lithospheric rebound over a low friction subduction fault [Giunchi et al., 1996]. Our study focused on the northern portion of the Calabria Arc, the Sila massif, to provide constraints on the long-term history of uplift and in turn, to the geodynamic evolution of the area.

[8] The Sila is a box-shaped massif characterized by a plateau standing at an average altitude of 1200 m a.s.l., representing an impressive relief in central Calabria. It is composed of Paleozoic intrusive and low to high-grade metamorphic rocks with a remnant of Mesozoic sedimentary cover [Ogniben, 1973; Amodio-Morelli et al., 1976; Dietrich, 1976; Lanzafame et al., 1979; Critelli, 1990] (Figure 1c). The massif is surrounded by low-standing basins filled by several Miocene–Holocene depositional sequences composed of poorly consolidated marine and fluvial conglomerate, sand and clay (Figure 1c) [Vezzani, 1968; Ogniben, 1973; Lanzafame and Tortorici, 1981; Colella et al., 1987; Critelli, 1990; Colella, 1995; Tortorici et al., 1995]. Along the eastern and southern borders of Sila, a Tortonian–Messinian clastic marine sequence unconformably lies on the Paleozoic bedrock, dipping outward with respect to the massif [Henderson,

1970; Guérémy, 1972; Bonardi *et al.*, 2005]. These deposits are unconformably overlain by upper Pliocene-lower Pleistocene transgressive marine deposits [Vezzani, 1968; Ogniben, 1973; Lanzafame and Tortorici, 1981; Colella *et al.*, 1987; Critelli, 1990; Colella, 1995; Tortorici *et al.*, 1995; Robustelli *et al.*, 2009]. Large Gilbert deltas, in the Crati R. valley, mark the progressive and strong sea level change during Pliocene-Holocene time [Colella, 1988]. Along the northern flank of the Sila the largest number of marine and alluvial terraces orders, including the remarkable MIS 5.5 terrace, have been recognized and mapped. Marine terraces have been associated from stages MIS 5.1, ca 80 ka in age, to stage MIS 11–9, ca 287–407 ka in age although the lack of numeric dating brings to uplift rates spanning between 0.4 to 1 mm/yr [Ciaranfi *et al.*, 1983; Amato and Cinque, 1999; Cucci and Cinti, 1998; Molin *et al.*, 2002; Carobene, 2003; Corbi *et al.*, 2009; Robustelli *et al.*, 2009]. In the Crotona region several marine terraces have been identified and correlated to stage from MIS 3 to MIS 7. The resulting average uplift rate spans between 0.8 and 1 mm/yr [Gliozzi, 1987; Cosentino and Gliozzi, 1988; Palmentola *et al.*, 1990; Zecchin *et al.*, 2004].

[9] The Sila Massif is bounded by straight flanks, locally related to recent faults (Figure 1c) [Colella, 1988; Tansi *et al.*, 2007; Robustelli *et al.*, 2009]. To the north, the basement units of the massif are separated from an upper Pliocene - upper Pleistocene coastal plain sequence by an E-W oriented, north-dipping normal to oblique-fault (Corigliano-Rossano fault) (Figures 1c and 4b) [Tortorici, 1981; Ciaranfi *et al.*, 1983; Knott and Turco, 1991; Moretti, 2000; Robustelli *et al.*, 2009]. The eastward continuation of this fault, the NW-SE oriented S. Nicola faults system, is retained to be active mainly during Miocene [Van Dijk *et al.*, 2000]. The eastern flank of the Sila decreases regularly toward the Crotona basin, without evidence of fault scarps while tectonic structures (i.e., Fuscaldo Mountains fault of Figure 4c) are concentrated within Crotona basin. The Sila southern flank is marked by a segmented, E-W oriented, fault system bounding the Catanzaro trough (Figures 1c and 4b) [Moretti, 2000; Faccenna *et al.*, 2011]. To the west, the Sila Massif topography slopes regularly but with steeper angle than eastern flank producing a general east-west asymmetric topography [Molin *et al.*, 2004]. The west flank decrease toward the Crati Valley, a N-S oriented extensional basin filled up by a Miocene-to-recent marine and continental sedimentary succession characterized on the west side by an important seismogenic faults system (West Crati faults System) (Figures 1 and 4b) [Tortorici, 1981; Lanzafame and Tortorici, 1981; Ghisetti and Vezzani, 1982; Colella, 1988; Colella *et al.*, 1987; Tortorici *et al.*, 1995; Moretti and Guerra, 1997; Cifelli *et al.*, 2007b; Spina *et al.*, 2011]. Along the eastern side of the Crati valley the occurrence of tectonic structures is limited to only two discontinuous faults system: the Piano Lago fault (Figure 1 and 4b), located in the high Crati valley is marked by morphological evidences and it is retained active [Galli and Bosi, 2003; Moretti, 2000]; the East Crati faults System (Figure 1 and 4b), located in the lower Crati Valley, providing few morphologic and field evidences has been constrained mainly by seismic profiles [Spina *et al.*, 2011]. Besides the most evident tectonic structures located along the basin surrounding the massif, two active faults cut the inner sector of the massif (Lake fault

and Cecita Lake fault) [Galli and Bosi, 2003;] showing normal to transtensional kinematics and trending NW-SE [Spina *et al.*, 2007] (Figure 4c). This faults system is retained active crosscutting Olocene deposits in the easternmost portion [Galli and Bosi, 2003]. The NNW-SSE directed Sellia-Decollatura faults system and the fault bounding southeastern massif margin do not have evidence of recent activity and probably constitute old and inactive structures [Bigi *et al.*, 1990; Van Dijk *et al.*, 2000].

[10] The exhumation history of the Sila Massif as constrained by apatite fission track analysis (AFT) that shows rapid cooling of the crystalline basement rocks between 35 Ma and 15 Ma as a result of crustal extension and subaerial erosion [Thomson, 1994, 1998].

[11] The Quaternary uplift of the Sila is recorded by flights of fluvial and marine terraces located in the Crati R. Valley and along the Ionian coast [Ciaranfi *et al.*, 1983; Colella *et al.*, 1987; Gliozzi, 1987; Cosentino and Gliozzi, 1988; Palmentola *et al.*, 1990; Cucci and Cinti, 1998; Molin *et al.*, 2002; Carobene, 2003; Zecchin *et al.*, 2004; Robustelli *et al.*, 2009; Ferranti *et al.*, 2009]. The uplift rates have been approximately calculated between 1 and 0.4 mm/yr [Gliozzi, 1987; Molin *et al.*, 2002; Carobene, 2003; Ferranti *et al.*, 2009].

3. Morphology of the Sila Massif

3.1. Methods

[12] We carried out geomorphological analysis and river longitudinal profile analysis over the entire Sila Massif using a 25 m resolution DEM coupled with field analysis. We analyzed the longitudinal river profiles to obtain information on the competition between rock uplift and erosion. In general terms, the progressive downstream decrease of the channel slope results in a smooth concave up shape that reflects lithologic uniformity and steady tectonic and climatic conditions [Mackin, 1948; Leopold *et al.*, 1964; Pazzaglia *et al.*, 1998].

[13] River longitudinal profiles can be described by an empirical power law relating local channel slope and drainage area taken as a proxy for discharge [Flint, 1974]:

$$S = k_s A^{-\theta} \quad (1)$$

where S is the local channel slope, A is the upstream contributing drainage area, and k_s and θ are morphological indices known as the steepness index and concavity index, respectively.

[14] Because θ and k_s could vary widely depending upon an assemblage of many factors, their significance and relation with tectonics, climate and lithology are still debated. Regardless, the relationship between k_s and rock uplift rate is widely accepted, although strongly influenced by geologic setting and climate [Wobus *et al.*, 2006, and references herein]. Uplift undoubtedly steepens rivers, and the steepness index should vary accordingly [Snyder *et al.*, 2000; Lague *et al.*, 2000; Schorghofer and Rothman, 2002; Dietrich *et al.*, 2003; Kober and Roering, 2004]. The concavity index spans a large range of values and its relationship to boundary conditions is ambiguous. Moderate values range between 0.4 and 0.7 have been found in rivers equilibrated to uniform moderate rock uplift rates. If lithology is

uniform, then low and high concavity indices may be associated with a downstream increase or decrease in incision rate, respectively. Extreme values (negative or >1) indicate strong differences in uplift rates in time or space and are usually associated with the formation of knickpoints [Whipple, 2004; Schoenbohm *et al.*, 2004; Hoke *et al.*, 2007].

[15] When a river is equilibrated with tectonic and climatic conditions, the river longitudinal profile may be modeled by a unique combination of k_s and θ values. If boundary conditions change, a river system assumes a transient state; its profile presents abrupt changes in channel slope that form convex reaches, called knickpoints. Knickpoints generated by a perturbation of the steady state tend to migrate headward. So equation (1) is a useful tool to extract information on regional tectonics and on uplift patterns [Kirby and Whipple, 2001; Wobus *et al.*, 2006].

[16] We conducted geomorphologic and morphometric analysis using ArcGIS to generate a hydrographic network and a free routine for MATLAB called Stream Profiler [Snyder *et al.*, 2000; Kirby *et al.*, 2003; Whipple, 2004; Wobus *et al.*, 2006] to extract and analyze stream long profiles, to generate log-log diagrams of slope versus area data, and to calculate steepness and concavity indices. We chose to remove spikes from river profiles by applying a smoothing window of 100 m and a contour interval of 25 m. In the slope versus area plots the linear regression was performed between the transition from steep debris flow dominated channels, marked by a nearly horizontal pattern of slope-area data, to fluvial channels, marked by linear slope-area scaling, and downstream to the bedrock-alluvial channel transition [Montgomery and Foufoula-Georgiou, 1993; Snyder *et al.*, 2000]. Moreover, knickpoints manually chosen at abrupt changes in channel slope have been used to separate stream profiles into segments. In order to extract the relative steepness and concavity indices, we performed the linear regression from the slope and drainage area data of these reaches.

[17] Because k_s and θ are autocorrelated [e.g., Sklar and Dietrich, 1998], we normalized the steepness index values (k_{sn}) by a reference concavity value of $\theta_{ref} = 0.4$, selected within theoretical range (0.3 to 0.6) [Hack, 1957; Howard *et al.*, 1994; Whipple and Tucker, 1999; Snyder *et al.*, 2000; Kirby and Whipple, 2001]. The normalized steepness values have been extracted following two procedures. In Method 1, they have been calculated for each river profile among the same regression limits of the concavity indices in order to matching directly the two values (Table 1) for the same river segment. In Method 2, the Stream Profiler tool generates automatically a map of steepness index by calculating the values of k_{sn} for short segments (0.5 km) of the all rivers in a catchment above a minimum drainage area, which we set to 10^6 m². This method allow to analyze all the rivers and to detect little variations along short segments unraveled by Method 1.

3.2. Results

[18] In plan view, the Sila Massif appears as a box-shaped relief with straight flanks, locally controlled by fault systems. The top of the Sila Massif is constituted by a low-relief upland surface, covering 600 km² and lying at an elevation of 1000–1600 m above sea level (Figures 2a and 2b). This high-standing landscape is characterized by small

plains and gently incised valleys which separate rolling topography 400–600 m higher than the valley bottoms (Figure 2b). The crystalline bedrock is strongly affected by weathering, which has generated saprolite up to a few tens of meters thick [Le Pera and Sorriso-Valvo, 2000]. Fluvial incision is very limited and weathering and areal erosion are the dominant processes presently affecting the upland landscape [Dramis *et al.*, 1990; Sorriso-Valvo, 1993]. Along the northeastern flank of Sila, Miocene shallow marine conglomerate deposits composed of rounded crystalline clasts crop out on the upland surface at a maximum elevation of 1200 m [Henderson, 1970; Sarti, 2010]. The high-standing surface has been interpreted as the relict of an old landscape formed at stable or slowly lowering base level conditions; indeed, it is only partially reached by the strong fluvial incision presently affecting the Sila flanks as a consequence of Quaternary uplift [Dramis *et al.*, 1990; Molin *et al.*, 2004]. The stream integration into the massif interior is still poor, and the abundance of wind gaps as well as some examples of fluvial piracy are representative of a still slowly developing landscape or of very recent deformation not yet pointed out by river longitudinal profiles or ¹⁰Be content. The extension of the shallow dipping surface envelope is marked in Figure 2a.

[19] The rolling topography of the perched relict landscape contrasts with the fluvial valleys that deeply incise the massif flanks. Wide valleys and very gentle channel slopes characterize streams flowing over the low-relief upland surface. Valleys get narrower and steeper as they cross the rim of the relict landscape, below which they expose bedrock with thin alluvial cover (Figure 2c). These valleys, characterized by steep slopes widely affected by landslides, cut down hundreds of meters with respect to the interfluves. The presence of step-pool and pothole channel bed morphologies are limited to very small reaches, and very steep knickpoints, such as waterfalls or rapids, have not been observed. Locally, fluvial strath terraces, rarely covered by a veneer of deposits, have been mapped out a few meters above seasonal flood level. Downstream, within Miocene to Quaternary basin deposits, river valleys get very wide and are filled with alluvial deposits (Figure 2d). The drainages are organized in a nearly radial pattern. The basins are elongated suggesting a very recent evolution [Molin *et al.*, 2004].

[20] We extracted the longitudinal profile of 35 rivers draining the entire Sila Massif (Figure 2a and Figure S1 in the auxiliary material), comprised of 29 main trunks and 6 tributary basins.¹ The river name, its concavity and steepness indices, and the minimum and maximum drainage areas of the regression limits are reported in Table 1. Figure 3 reports one representative river profile for each massif flank. Most of the studied rivers exhibit longitudinal profiles far from the smooth concave up shape typical of streams in equilibrium conditions. Conversely, they exhibit knickpoints or knickzones, separating reaches with different morphometric parameters (Figures 3 and 4). The distribution of knickpoint elevations shows two maxima at around 1100 m and at 800 m a.s.l. (Figure 4c). Field

¹Auxiliary materials are available in the HTML. doi:10.1029/2011TC003037.

Table 1. Results of Morphometric Analyses of the Sila Rivers

Name	River Number	Segment	Amin (km ²)	Amax (km ²)	$\theta \pm 2\sigma$ (θ) ^a	ksn ^b \pm ksn2 σ
Coriglianeto	1	1	0.01	0.4	0.27 \pm 0.33	5.7 \pm 13.46
Coriglianeto	1	2	0.59	20.75	0.31 \pm 0.14	26.5 \pm 25.2
Coriglianeto	1	3	26.9	51.93	0.02 \pm 1.04	37.35 \pm 34.48
Cino	2	1	0.03	15.82	0.34 \pm 0.14	18.08 \pm 19.18
Cino	2	2	14.53	21.47	-4.19 \pm 2.6	63.87 \pm 72.8
Cino	2	3	22.98	43.06	2.12 \pm 0.84	47.34 \pm 51.15
Colognati	3	1	0.04	6.88	0.43 \pm 0.07	30.11 \pm 30.94
Colognati	3	2	6.43	20.06	-0.92 \pm 0.64	63.23 \pm 69.2
Colognati	3	3	17.22	53.7	2.2 \pm 0.4	38.68 \pm 43.42
Coserie	4	1	0.02	0.96	0.39 \pm 0.11	22.48 \pm 23.45
Coserie	4	2	1.65	6.11	1.08 \pm 0.39	54.33 \pm 63.52
Coserie	4	3	8.73	84.92	0.96 \pm 0.31	30.47 \pm 32.23
Trionto	5	1	0.02	25.44	0.21 \pm 0.14	5.01 \pm 5.69
Trionto	5	3	70.46	293.28	0.69 \pm 0.24	55.2 \pm 44.28
Ortiano	6	1	0.68	55.51	0.39 \pm 0.1	47.61 \pm 48.37
Laurenzana	7	1	0.24	8.3	0.29 \pm 0.15	35.12 \pm 36.63
Laurenzana	7	2	7.49	14.28	-0.58 \pm 1.77	38.08 \pm 41.11
Laurenzana	7	3	12.9	105.9	0.72 \pm 0.22	32 \pm 33.32
Lese	8	1	1.01	11.65	0.84 \pm 0.44	16.54 \pm 19.81
Lese	8	2	19.13	53.58	0.49 \pm 1.2	34.62 \pm 38.89
Lese	8	3	53	172.96	0.04 \pm 0.57	56.16 \pm 58.29
Lese trib1	9	1	7.75	20.06	0.35 \pm 0.12	48.98 \pm 50.84
Lese trib1	9	3	21.37	46.42	0.01 \pm 0.76	51.92 \pm 56.98
Lese trib2	10	1	0.17	1.08	0.76 \pm 0.63	27.59 \pm 33.92
Lese trib2	10	2	1.57	7.49	1.2 \pm 0.38	29.9 \pm 35.07
Lese trib2	10	3	7.88	15.55	0.19 \pm 1.27	48.99 \pm 51.86
Neto	11	1	0.01	82.09	0.39 \pm 0.17	5.18 \pm 6.96
Neto	11	2	71.66	205.33	-2.24 \pm 1.27	39.77 \pm 44.73
Neto	11	3	288.34	456.02	2.39 \pm 1.8	90.62 \pm 95.39
Neto trib	12	1	0.07	86.81	0.55 \pm 0.08	16.09 \pm 17.84
Neto trib	12	2	76.7	115.28	-6.71 \pm 5.56	48.43 \pm 52.93
Ampollino	13	1	0.17	61.74	0.79 \pm 0.11	11.87 \pm 16.93
Ampollino	13	2	61.74	75.13	-2.29 \pm 3.05	106.69 \pm 110.41
Tacina	14	1	0.02	16.93	0.46 \pm 0.08	8.94 \pm 9.68
Tacina	14	2	32.27	55.55	2.48 \pm 2.06	57.27 \pm 62.88
Tacina	14	3	47.31	81.89	0.27 \pm 1.56	82.22 \pm 85.2
Soleo	15	1	0.13	6.32	-0.07 \pm 0.08	7.47 \pm 11.72
Soleo	15	2	6.88	16.93	0.36 \pm 1.31	59.08 \pm 66.99
Soleo	15	3	30.56	46.64	-0.11 \pm 1.41	85.5 \pm 87.56
Mesoraca	16	1	0.08	3.32	0.34 \pm 0.15	27.09 \pm 28.16
Mesoraca	16	2	4.16	21.39	0.57 \pm 0.52	51.54 \pm 54.25
Mesoraca	16	3	21.38	26.66	-1.98 \pm 3.68	93.67 \pm 97.11
Crocchio	17	1	0.02	1.96	0.12 \pm 0.66	27.72 \pm 35.39
Crocchio	17	2	1.96	8.5	-0.2 \pm 0.16	50.96 \pm 53.52
Crocchio	17	3	10.34	48.5	-0.03 \pm 0.56	80.34 \pm 83.49
Simeri	18	1	0.24	20.75	0.38 \pm 0.08	13.32 \pm 13.83
Simeri	18	3	21.33	58.58	-0.07 \pm 0.45	83.92 \pm 87.15
Simeri trib	19	1	0.87	7.24	0.03 \pm 0.28	59.87 \pm 62.66
Forestale	20	1	0.22	2.06	0.23 \pm 0.31	20.54 \pm 23.09
Forestale	20	2	2.72	11.01	0.45 \pm 0.53	71.95 \pm 73.89
Forestale	20	3	11.11	29.72	0.9 \pm 0.62	52.84 \pm 57.2
Alli	21	1	0.14	25.01	0.46 \pm 0.15	8.19 \pm 9.16
Alli	21	2	29.47	38.51	-7.88 \pm 5.12	52.27 \pm 64.3
Alli	21	3	39.08	89.72	1.47 \pm 0.63	54.49 \pm 58.21
Melito	22	1	0.05	8.16	0.61 \pm 0.14	11.53 \pm 13.46
Melito	22	2	10.92	37.88	1.15 \pm 0.45	29.85 \pm 32.91
Melito	22	3	38.36	40.9	-145.49 \pm 170.15	177.29 \pm 199.01
Corace	23	1	0.01	0.99	0.41 \pm 0.19	16.27 \pm 18.22
Corace	23	2	1.35	60.47	0.88 \pm 0.11	18.14 \pm 20.18
Corace	23	3	107.46	172.07	1.27 \pm 2.35	63.6 \pm 71.77
Amato	24	2	1.38	69.63	0.99 \pm 0.33	8.42 \pm 12.25
Amato	24	3	76.02	109.1	-1.33 \pm 2.5	47.8 \pm 50.09
Savuto	25	1	0.12	68.62	0.38 \pm 0.13	13.96 \pm 14.78
Savuto	25	2	68.61	80.96	12.35 \pm 3.12	93.29 \pm 105
Savuto	25	3	118.68	201.85	0.7 \pm 2.33	46.28 \pm 50.01
Craticello	26	2	0.02	5.71	0.2 \pm 0.11	28.97 \pm 32.18
Craticello	26	3	5.89	99.6	0.79 \pm 0.15	55.26 \pm 58.66
Cardone	27	2	0.03	6.17	-0.02 \pm 0.17	21.75 \pm 25.17
Cardone	27	3	6.19	50.4	0.76 \pm 0.17	65.02 \pm 67.16
Padula	28	2	0.01	6.98	0.24 \pm 0.07	28.1 \pm 29.65
Corno	29	2	0.01	0.81	0.29 \pm 0.18	31.58 \pm 33.31
Corno	29	3	0.77	10.94	0.07 \pm 0.18	49.29 \pm 51.57

Table 1. (continued)

Name	River Number	Segment	Amin (km ²)	Amax (km ²)	$\theta \pm 2\sigma$ (θ) ^a	ksn ^b \pm ksn2 σ
Arente	30	2	0.02	17.51	0.35 \pm 0.07	36.87 \pm 37.98
Arente	30	3	47.31	69.85	-0.02 \pm 2.5	61.08 \pm 64.95
Gidora	31	2	0.02	4.13	0.29 \pm 0.09	49.09 \pm 50.64
Gidora	31	3	8.47	11.82	1.73 \pm 1.43	46.08 \pm 48.78
Mucone	32	1	0.1	30.96	0.29 \pm 0.13	25.74 \pm 27.01
Mucone	32	2	193.81	217.49	12.75 \pm 8.67	80.44 \pm 91.21
Mucone	32	3	226.42	298.11	-0.19 \pm 2.32	55.73 \pm 58.85
Duglia	33	1	0.02	5.91	0.42 \pm 0.26	13.3 \pm 16.2
Duglia	33	3	5.67	56	-0.14 \pm 0.32	36.09 \pm 38.47
Galatrella	34	1	0.06	2.62	0.55 \pm 0.16	18.78 \pm 20.55
Galatrella	34	2	2.49	4.58	-0.78 \pm 3.55	26.09 \pm 30.42
Galatrella	34	3	5.71	40.16	0.52 \pm 0.26	21.92 \pm 23.15
Mizofato	35	1	0.06	3.49	0.47 \pm 0.12	33.74 \pm 35.36
Mizofato	35	3	4.21	26.77	1.03 \pm 0.54	29.63 \pm 31.48

^aBest-fit channel concavity.

^bNormalized channel steepness index calculated using $\theta_{\text{ref}} = 0.40$.

analysis confirms that knickpoints are not related to changes in susceptibility to erosion or in rock type.

[21] In spite of their variability, river profiles share some common features: 23 among the 35 analyzed river profiles rise within the high-standing landscape and they are characterized by a higher, flat reach bounded downstream by a major knickpoint (herein referred as first knickpoint) that marks the edge of the upland surface (type A). The remaining 12 river profiles rise along the outer massif flanks and lack an upper flat segment (type B). In addition, most of the rivers (29 among 35), regardless of their source location rising point, show an intermediate major knickpoint (type *). In the rivers that originate from the upland surface, the presence of an intermediate knickpoint produce a three-segment profile (A*), composed by an upper flat reach, an intermediate steep reach, and a lower reach. The intermediate reach, downstream of major knickpoints, shows a variable shape that can be characterized by either a concave-up shape (9 rivers) or by a wide knickzone (20 rivers). For the rivers rising only along the flanks, the intermediated knickpoint separates an upper steep reach from a lower reach (B*). Downstream of the second knickpoint, the lower reach, which shows a straight or convex shape, extends for several hundreds of meters in elevation, starting from 600 to 700 m a.s.l., down to the transition to alluvial channels and does not correspond to variations in lithology, basin drainage area or to tectonic structures.

[22] The profiles of four rivers that have their source in the upland are characterized by only one knickpoint (river n5, 18, 21, 33, type A) that bounds the upper flat reach, downstream of which occurs an apparently equilibrated profile without knickpoints. The majority of the rivers draining the western flank of the massif lack the flat segment at their heads and can be categorized in B*. Indeed, with the exception of the Duglia River (n33) and Mucone River (n32) which drains a large portion of the high-standing low-relief topography, these westward draining rivers are not integrated into the old landscape. Instead, they all show the second knickpoint and discernable short rectilinear lowermost reach.

[23] The values of concavity index for river reaches draining the upland relict landscape range from 0.3 to 0.6, attaining typical values for longitudinal profiles close to

equilibrium conditions. The intermediate segments display a relatively wide range of concavity indices (from -7.88 to 12.75). The concavity index of lower reaches fall in a wide range of values (from -0.14 to 2.2). The values lower than 0.3 are consistent with the straight/convex reach shape. In general, low concavity indices distinctly mark lowermost reaches of the rivers (Figure 2). A particular case is represented by the Crocchio River, in the southeastern tip of the massif, because it is characterized by negative concavity index for the whole length of the profile (Figure 3c).

[24] Steepness values have been calculated by two methods. By Method 1 the steepness is calculated along each morphological river segment and it can be compared with the concavity index over the same river segment. The values of steepness index are normalized by reference concavity value of $\theta_{\text{ref}} = 0.4$, and reported in the Table 1. Method 2 allows us to distinguish little variation on steepness index in the order of 50 m and can be calculated for the all of the rivers. The steepness values extracted by Method 2 are displayed in the map of Figure 4. This map reveals a distinct spatial pattern: high values constitute a belt around the edge of the upland relict landscape, marking the transition to the modern deeply incised landscape of the Sila flanks. Along this belt, the normalized steepness indices vary from 50 to 232, reaching the highest values in the southeastern portion of the massif. Moreover steepness index spatial distribution (Figure 4b) shows a good correspondence between local high values and some active tectonic structures, as Corigliano-Rossano fault, Catanzaro fault, East Crati fault and Piana Lago fault. In the upland relict landscape the rivers are definitely less steep with index values lower than 50, values typical of alluvial reaches.

4. Cosmogenic Analysis

4.1. Methods

[25] We determined catchment-averaged erosion rates from the concentrations of cosmogenic beryllium-10 (¹⁰Be) in quartz-bearing alluvial sediments. Beryllium-10 accumulates in quartz near the Earth's surface proportional to its local production rate and inversely proportional to the surface erosion rate [e.g., von Blanckenburg, 2005]. The cosmogenic nuclide method averages erosion rates over the time required

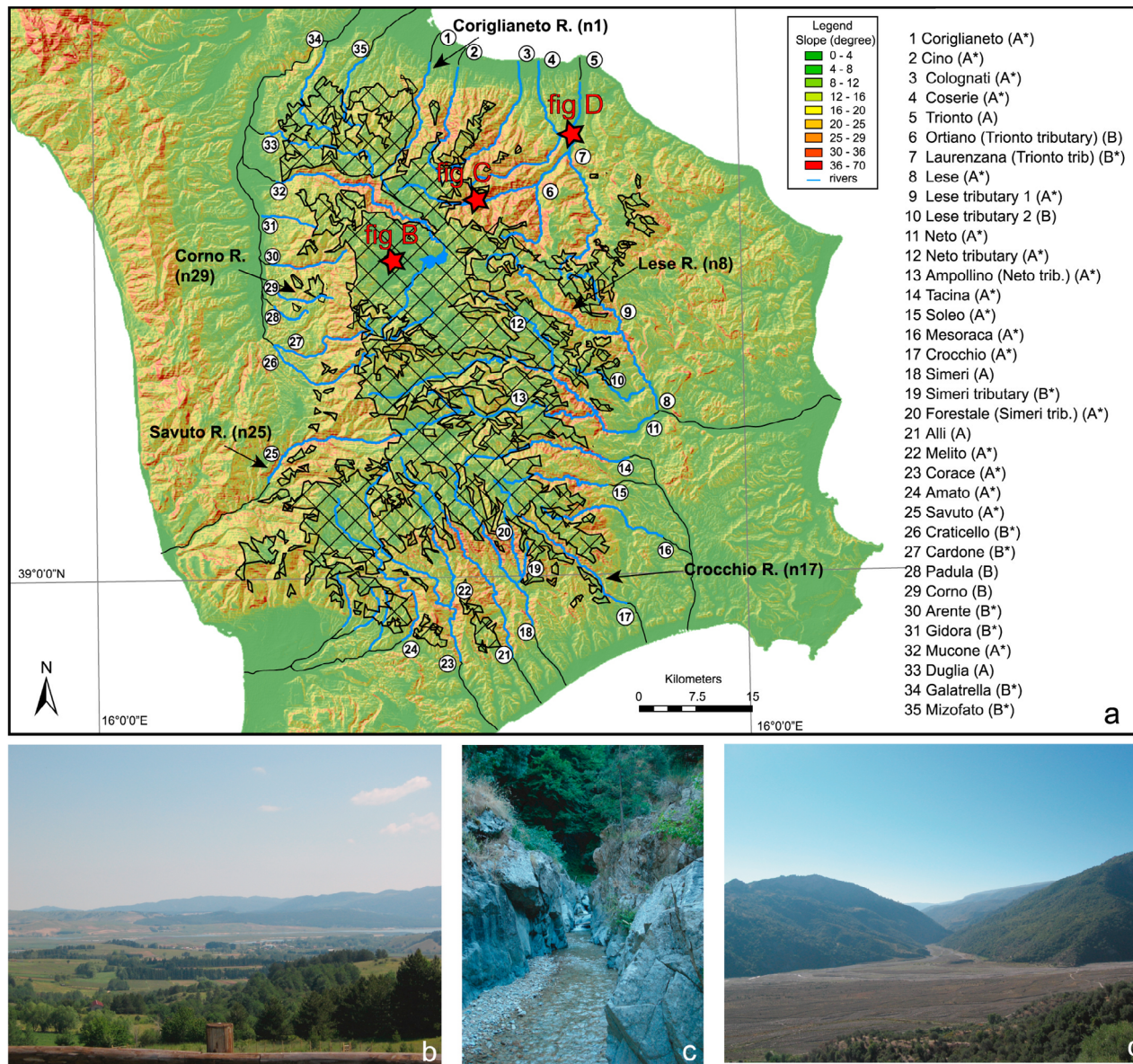


Figure 2. (a) Slope map of the Sila Massif. Rivers analyzed are traced in blue, rivers not analyzed in black. Patterning polygons represent a low slope area ($<5^\circ$) covering crystalline rocks with an altitude > 200 m a.s.l. Low slope areas of Miocene deposits and valley bottoms have been ruled out. Stars indicate locations of the pictures. The name of the rivers with relative identification number is shown. Letter in parentheses corresponds to river type: (A) river rising within the upland, (B) river rising along the flank, (*) river with intermediate knickpoint. **(b)** View of the low-relief upland developed on the top of Sila Massif. **(c)** An example of one incised valley reach looking upstream of the Trionto River. **(d)** View to the east (upstream) of the incised broad valley of the Trionto River at the confluence of its main tributary Laurenzana River. Low-relief upland surface can be seen in the far distance.

to erode one cosmic ray penetration length, or ~ 60 cm in rock of density 2.6 g/cm^3 [Lal, 1991; Masarik and Reedy, 1995]. In most landscapes this is anywhere from 10^3 to 10^5 years.

[26] In order for ^{10}Be concentrations to accurately indicate catchment-averaged erosion rates, several conditions must be met. Quartz must be uniformly distributed within the catchment, or else erosion rates will be biased toward areas with higher quartz content. Sediment samples must be representative of the entire watershed, as opposed to being

dominated by a single landslide. If erosion does occur primarily by landsliding, then the catchment should be large enough that a sample of sediment is likely to contain grains from many different landslides [Niemi et al., 2005; Yanites et al., 2009]. The catchment should not have been glaciated, because glaciation may disrupt sediment transport paths, making stream sediment unrepresentative of the catchment as a whole [von Blanckenburg, 2005; Wittmann et al., 2007; Stock et al., 2009]. Finally, erosion must

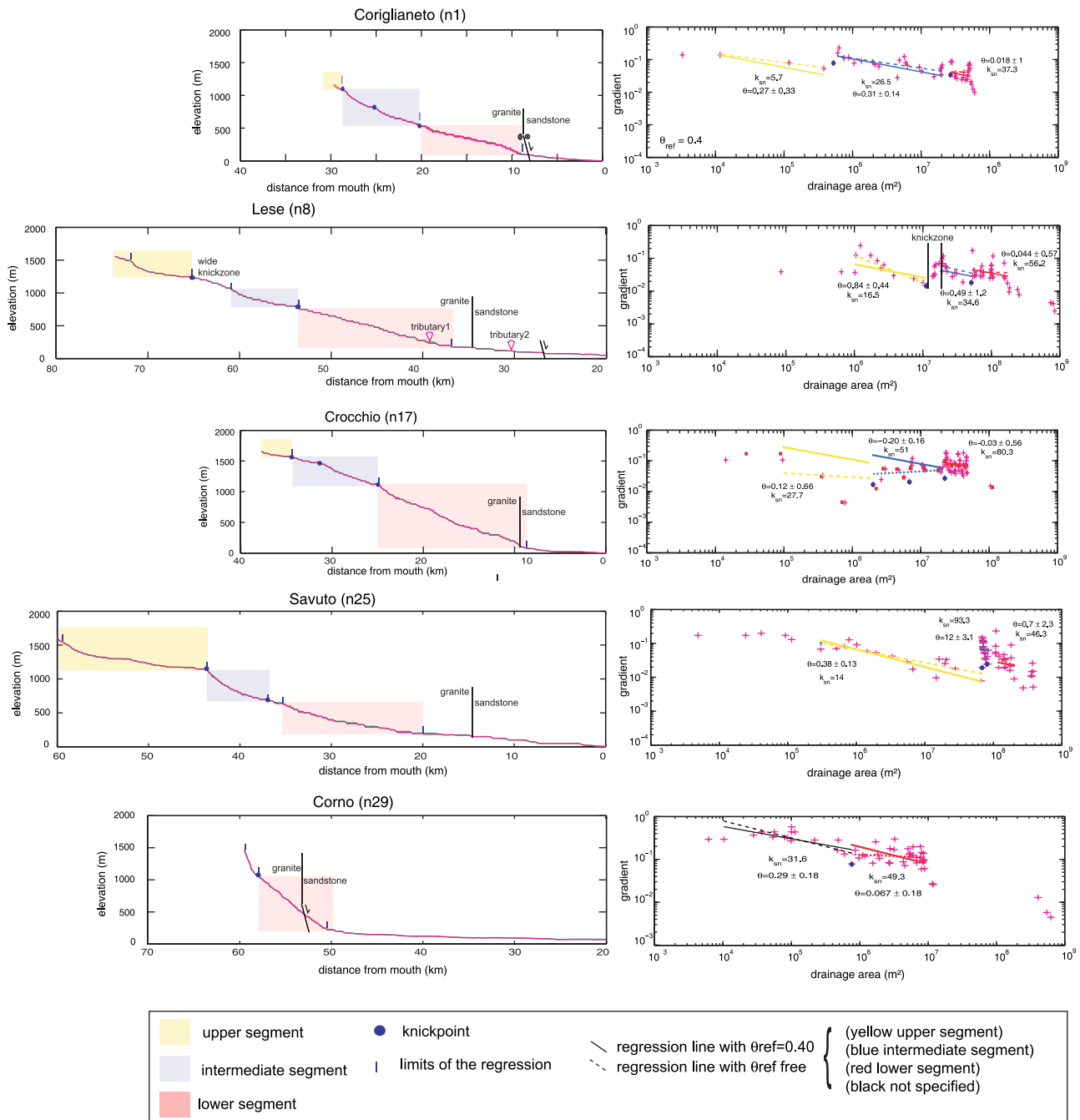


Figure 3. Longitudinal profiles and area-slope plots relative to five rivers, each representative of a flank of the massif (see locations in Figure 2a). Colored squares evidence the main three segments of river longitudinal profiles. The rest of the profile analysis is in the auxiliary material.

occur at a nearly constant rate over the time taken to erode through several secondary cosmic ray penetration lengths (a few meters). If erosion rates have changed through time, then ^{10}Be concentrations will provide an average erosion rate [Schaller and Ehlers, 2006].

[27] We calculated catchment-averaged erosion rates from ^{10}Be concentrations in quartz-bearing alluvial sediments [von Blanckenburg, 2005]. We collected 24 samples from 7 different catchments from either the active channel or from fluvial sediment in freshly exposed sandy bars. In each of

these 7 catchments, we collected sediment at the bottoms of upstream flat reaches draining the low-relief upland of the Sila, from one or more locations along the middle reach, and from just upstream of the transition from bedrock-dominated to fully alluviated stream channels. We also collected sediment from major tributaries in three catchments (Trionto, Lese, and Simeri Rivers), sampling from just upstream of channel confluences. Quartz was physically separated from the 0.5 to 1.0 mm size fraction, and ^{10}Be chemically isolated

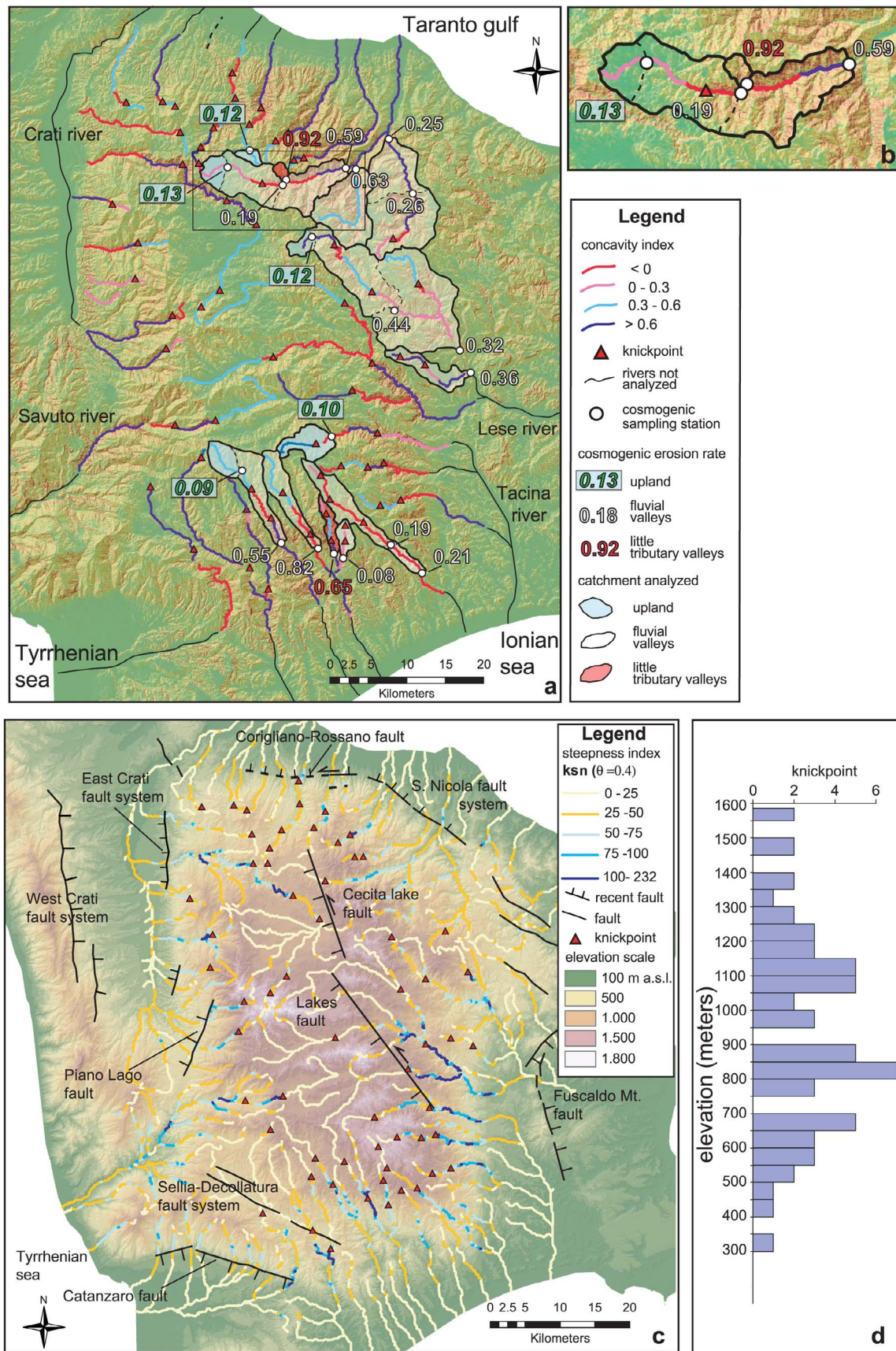


Figure 4

Table 2. Cosmogenic Nuclide Data

Sample Name	Quartz Mass (g)	[¹⁰ Be] 10 ³ (at/g) Quartz ^a	Production Rate Catchment Average ^b (at/g)	Erosion Rate Catchment Average ^c (mm/yr)
Cino	116,999	68 ± 5.1	11.6 ± 0.81	0.1 ± 0.01
Trionto 1b	79,528	68.4 ± 4.5	11.8 ± 0.83	0.13 ± 0.01
Trionto 3 (Laurenzana)	202,857	26.1 ± 1.8	8.9 ± 0.62	0.25 ± 0.02
Trionto 4 (Laurenzana)	175,470	26.8 ± 1.7	9.7 ± 0.68	0.26 ± 0.02
Trionto 5 (Ortiano)	226,920	12.1 ± 1.3	10.7 ± 0.75	0.63 ± 0.07
Trionto 6	607,275	14.3 ± 0.6	11.9 ± 0.83	0.57 ± 0.04
Trionto 7 (no name trib)	209,152	10.2 ± 0.7	13.3 ± 0.93	0.92 ± 0.08
Trionto 8	389,670	48.3 ± 1.9	12.4 ± 0.87	0.19 ± 0.01
Lese 1	265,800	18.7 ± 1.3	11.7 ± 0.82	0.44 ± 0.04
Lese 3	330,112	91.5 ± 4.6	16.1 ± 1.13	0.12 ± 0.01
Lese 5	459,279	22.6 ± 3.1	10.1 ± 0.71	0.32 ± 0.04
Lese 6 (Lese Trib2)	202,796	14.8 ± 1.3	10.2 ± 0.71	0.36 ± 0.05
Tacina	167,210	114.3 ± 4.1	16.3 ± 1.14	0.1 ± 0.01
Crocchio 1	572,784	52.4 ± 2	14.5 ± 1.02	0.19 ± 0.01
Crocchio 2	617,219	43.2 ± 1.6	12.7 ± 0.89	0.21 ± 0.01
Simeri 1	252,866	19.5 ± 3	10.5 ± 0.74	0.38 ± 0.05
Simeri 3	168,437	11.6 ± 1	13.6 ± 0.95	0.82 ± 0.08
Simeri Trib	305,372	100.2 ± 3	10.9 ± 0.76	0.08 ± 0
Forestale 1	169,965	12.2 ± 1.1	11.3 ± 0.79	0.65 ± 0.06
Alli 1	300,507	106.3 ± 3.4	13.4 ± 0.94	0.09 ± 0.01
Alli 2	366,016	15.9 ± 0.9	12.5 ± 0.88	0.55 ± 0.04

^a¹⁰Be measured by accelerator mass spectrometry at PRIME Lab, Purdue University, against standards prepared by K. Nishiizumi. Concentrations have been decreased by 14% to correct for a ¹⁰Be half-life of 1.34 Myr [Nishiizumi et al., 2007].

^bProduction rate is the spatially averaged production rate over the catchment, scaled for elevation and latitude according to Stone [2000], using a sea-level, high-latitude production rate of 5.1 at/g quartz/yr decreased by 14% based on a ¹⁰Be half-life of 1.34 Myr [Nishiizumi et al., 2007].

^cQuoted uncertainty is the analytical uncertainty only and does not include a ~7% uncertainty in the sea-level, high-latitude ¹⁰Be production rate.

from that quartz, according to the standard operating procedures of PRIME Lab. Beryllium-10 concentration was determined from ¹⁰Be/⁹Be, measured at PRIME Lab against standards prepared by K. Nishiizumi [Nishiizumi et al., 2007].

[28] We calculated catchment-averaged erosion rates, ϵ , from the concentrations of ¹⁰Be, N , according to [Granger et al., 2001]

$$N = \frac{P_n}{(1/\tau + \rho\epsilon/\Lambda)} + \frac{P_{\mu 1}}{(1/\tau + \rho\epsilon/L_1)} + \frac{P_{\mu 2}}{(1/\tau + \rho\epsilon/L_2)} + \frac{P_{\mu 3}}{(1/\tau + \rho\epsilon/L_3)}, \quad (2)$$

where P_n , $P_{\mu 1}$, $P_{\mu 2}$, and $P_{\mu 3}$ are the production rates of ¹⁰Be by spallation and muon processes (at/g quartz/yr), τ is the radioactive mean life of ¹⁰Be (yr⁻¹), ρ is the material density (g/cm³), Λ is the attenuation length for ¹⁰Be production by spallation (g/cm²), and L_1 , L_2 and L_3 are the attenuation lengths for ¹⁰Be production by muon reactions (g/cm²). We calculated ¹⁰Be production rates as an area-weighted catchment-averaged production rate scaled from sea level,

high latitude according to Stone [2000] using the constants from Granger and Smith [2000].

4.2. Results

[29] Erosion rates calculated from cosmogenic ¹⁰Be concentrations are presented in Figure 4a and Table 2. Catchment-averaged erosion rates in the Sila massif reveal an order-of-magnitude variation between the upland surface and the incised valleys (Figure 4a and Table 2). The overall pattern shows erosion rate values that are lower in the upland and increase downstream before slightly decreasing in the low-ermost segments (Figure 4a and Table 2). Indeed, samples collected on the low-relief high-standing landscape (italic in Figure 4a) show erosion rates between 0.09 ± 0.01 and 0.13 ± 0.01 mm/yr. Conversely, samples collected along the massif flanks show a large range of erosion rates, with values between 0.08 ± 0.01 to 0.92 ± 0.08 mm/yr. This wider range could be related to different processes delivering sediment from hillslopes to stream channels. For example, the Simeri River and one of its tributaries, both of them draining only the flank of the Sila Massif, have completely different erosion rates (0.08 ± 0.01 and 0.82 ± 0.08 mm/yr). Also, the erosion rates from samples collected along the Crocchio River, which is characterized by a convex longitudinal profile and a poorly

Figure 4. (a) Slope map of the Sila Massif showing the distribution of best fit concavity indices for the rivers analyzed. Note that the lower reaches tend to have low concavities (red and pink colored), whereas the upper segments show moderate values. Numbers indicate ¹⁰Be catchment-averaged erosion rates in mm/yr (circles indicate sample location); the limits of the relative catchment are shown. (b) Particular of the high Trionto River valley where erosion rates have been deconvolved by the different contributions areas. (c) Topographic map of the Sila Massif showing the distribution of normalized steepness indices calculated for short segments (0.5 km) of all rivers with drainage area larger than 10⁶ m². Tectonic features from Tortorici et al. [1995], Galli and Scionti [2006], and Bigi et al. [1990]. (d) Histogram of knickpoint elevation. Note the clustering at around 800 and 1100 m of elevation.

incised valley, are anomalously low relative to other samples collected along the massif flanks. In contrast, erosion rates as high as 0.92 ± 0.08 mm/yr and 0.65 ± 0.06 mm/yr are observed in small tributary catchments developed only within the massif flank (Trionto7 and Forestale1 respectively).

5. Discussion

[30] Quantifying rock uplift rates, hillslope erosion rates, and the fluvial longitudinal profile morphology are all possible methods of investigating mountainous landscape evolution. However, the utility of these tools is limited by our incomplete knowledge of how these different processes interact to produce a non-transient landform. Most of the uncertainties derives from a poor understanding of the timescale of landform response to a change in the rate of rock uplift (base level fall).

[31] As a way to address this issue, we concentrated our analysis on a key site, the Sila massif, a small but lithologically homogenous structure interested by relevant uplift rate. We used cosmogenic ^{10}Be to measure basin-scale erosion rates, and river profile analysis to unravel the interplay between transient landscape evolution and tectonic uplift. Our main results can be summarized as follows.

[32] 1. Cosmogenic ^{10}Be data show a large variation in erosion rates but can be divided into three main domains. The highest elevation, low-relief domain shows low erosion rates, between 0.09 ± 0.01 and 0.13 ± 0.01 mm/yr. High erosion rates, up to 0.92 ± 0.08 mm/yr, characterize the incised fluvial valleys on the flanks of the massif. In the lower portions of the rivers, erosion rates show medium values, between 0.25 ± 0.02 and 0.36 ± 0.05 mm/yr.

[33] 2. The majority of river longitudinal profiles are characterized by three segments separated by two major knickpoints. The highest reach, located on the low-relief surface atop Sila, is smooth, concave-up, and characterized by concavity indices between 0.3 and 0.6 and low values of k_{sn} . The downstream limit of this highest segment, the “first” knickpoint, is located at the boundary between the old upland landscape and the Sila flanks. The second, shorter, stream profile segment shows a variable profile from a concave-up to straight or even convex-up shape and is bounded at the downstream end by the “second” knickpoint. Here steepness indices are higher than anywhere else on the Sila, and concavity indices are between -7.88 and 12.75 . Below this second knickpoint, the third stream segment shows a rectilinear profile, and has moderate steepness indices and concavity indices between 0.14 and 2.2.

[34] The low-relief landscape on top of Sila, where normalized steepness indices are low, represents a relict landscape probably developed during stable or slowly lowering base level conditions [Dramis *et al.*, 1990; Molin *et al.*, 2004; Scarciglia *et al.*, 2005]. This landscape is not yet reached by the headward fluvial incision presently affecting the Sila flanks. Accordingly, cosmogenic ^{10}Be erosion rates are low and comparable to the highest erosion rates reported from tectonically stable areas [Schaller *et al.*, 2002; von Blanckenburg, 2005]. Outside of the upland surface, on the Sila Massif flanks, the steeper river profiles show distinct signs of tectonic perturbation as they are characterized by two major knickpoints.

[35] The upper, first, knickpoint marks the abrupt change in channel slope and steepness index from the flat reach on top of the Sila to the deeply incised fluvial valleys on the massif. It represents a regressive wave of incision that, migrating upstream in response to uplift, has isolated the low-relief landscape on top of the Sila and has generated a river profile now represented by the intermediate reach. This is bounded downstream by the second knickpoint, which could be interpreted as a record of a subsequent regressive wave of incision produced by a change in regional uplift rate. This variation is indicated by the different values of concavity index between the lowermost and the intermediate reaches. Indeed, detachment-limited river incision models predict that steepness and concavity indices tend to be equilibrated with uplift rate, such that changes in index values indicate channels equilibrated to different uplift rates [Stock and Montgomery, 1999; Kirby and Whipple, 2001; Wobus *et al.*, 2006]. Finally, the rectilinear channel segment below the second knickpoint indicates that fluvial incision rates are slower than the present-day uplift rate.

[36] Cosmogenic ^{10}Be erosion rate data along the river valleys show faster erosion rates on the Sila massif flanks with respect to erosion rates of the relict landscape, consistent with the transient condition of the whole massif. The cosmogenic erosion rates along the river valleys display a large variability, from 0.08 ± 0.01 to 0.92 ± 0.08 mm/yr. The erosion rates of 0.92 ± 0.08 mm/yr of sample Trionto 7 and 0.65 ± 0.06 of Forestale, a Simeri tributary, come from a small tributary basin developed only within the massif flank, and located beneath the unique knickpoint and the second knickpoint respectively. For these reasons these values are probably closer to the “true” erosion rate acting on the modern landscape represented by the Sila massif flanks. Lower erosion rates of 0.13 ± 0.01 and 0.19 ± 0.01 , from the main stem of the Trionto River upstream of the confluence with the sampled tributary basin, probably reflect mixing of sediment coming from the low-relief upland surface and sediment coming from other small tributary catchments to the Trionto. Based on a two-end-member mixing model, we calculate the proportion of sediment from the upland landscape of the Sila relative to the amount of sediment contributed from the massif flanks at the location Trionto 8, just below the first knickpoint, where the erosion rate is 0.19 ± 0.01 . Based on this model, 94% of sediment is sourced from the relict landscape (0.13 ± 0.01 mm/yr) and 6% of sediment from the modern landscape (0.92 ± 0.08 mm/yr). This proportion changes downstream, with an increase in the amount of sediment supplied from the rapidly eroding massif flanks. Therefore in the intermediate reach of the Trionto river, cutting across the modern landscape, the erosion rate increases at 0.59 ± 0.04 mm/yr (sample Trionto 6). This is caused by the increased contribution of sediment from the rapidly eroding massif flanks that reach the 53% of the entire sediment supply.

[37] In the lower portions of the rivers the cosmogenic ^{10}Be erosion rates, even though far from the relict upland, decrease relative to erosion rates in the middle parts of catchments. We interpret this as an increased contribution of sediments from slowly eroding landscape fragments located on interfluvies at low altitude [Molin *et al.*, 2002]. An example is from the Simeri River tributary (sample named

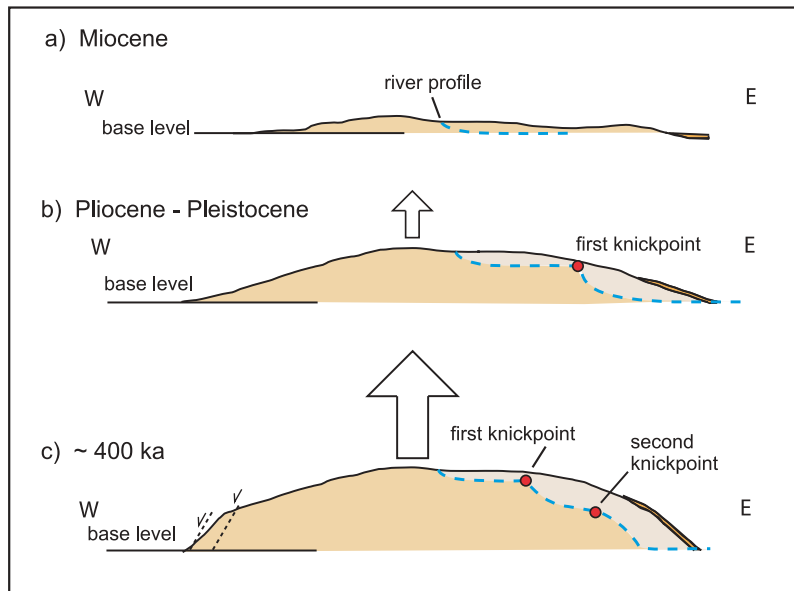


Figure 5. Schematic diagram showing the uplift history of the Sila massif. (a) Formation of a low-relief landscape during a long lasting period of limited or slow uplift balanced by erosion. Crystalline rocks of the Sila contribute to clastic deposits along the neighboring basins. (b) First increase in uplift rate produces the first knickpoint and isolates the low-relief landscape. (c) Second increase in uplift rate leads to the formation of the second knickpoint and consequent lower fluvial segment characterized by a rectilinear to convex shape. The increased uplift rate is amplified by normal fault activity.

Simeri Trib), which has a very low erosion rate of 0.08 ± 0.01 mm/yr.

[38] Although this small catchment is restricted to the massif flank, it is mainly constituted of low-gradient hill-slope ($<5^\circ$), with a minor proportion of high-gradient hill-slope area. This erosion rate may indicate that patches of low eroding surface not yet reached by the present headward fluvial incision stand at low altitude along the massif flanks. We propose that this slow eroding surface corresponds to relict surface, maintaining a topographic continuity from the upland atop the massif. Here, the large variation in cosmogenic ^{10}Be erosion rates and non-equilibrated river profiles indicate a disequilibrium state related to a strong uplift not yet counterbalanced by erosion.

5.1. Tectonic Implications

[39] River profile analysis and cosmogenic ^{10}Be erosion rate data provide constraints on the evolution of the landscape, but the age of the relict landscape and timing of the onset of uplift remain a matter of debate. In this section we try to integrate our data with geological and geochronological constraints to unravel the evolution of the Sila landscape.

[40] Cosmogenic ^{10}Be erosion rates from the upland surface are low (0.09 ± 0.01 to 0.13 ± 0.01 mm/yr) and, although they are effective for the last 10^4 yr, indicate that the relict landscape preserves the pre-uplift erosion rates. This is supported by the observation that the regressive stream incision has not reached the low-relief upland, based on the position of the first knickpoint. Moreover, the low erosion rates are similar to denudation rates from apatite fission track thermochronology, which shows denudation rates of 0.1–0.2 mm/yr over the last 15–20 Ma [Thomson, 1994]. The presence of Sila crystalline rock clasts in Tortonian continental and marine sediments in

the basins surrounding Sila [Ogniben, 1973; Amodio-Morelli et al., 1976; Ortolani et al., 1979; Romeo and Tortorici, 1980; Sorriso-Valvo and Sylvester, 1993; Colella, 1995; Argentieri et al., 1998; Critelli and Le Pera, 1998] indicates a middle Miocene emersion of the present upland surface, which probably underwent a slow base level lowering and allowed the development of a low-relief landscape [Molin et al., 2004]. Moreover, the weathering of the upland surface resulting in saprolite tens of meters thick [Matano and Di Nocera, 1999; Le Pera and Sorriso-Valvo, 2000; Scarciglia et al., 2005], and the smooth concave geometry of river longitudinal profiles, are consistent with the antiquity of the relict landscape.

[41] After a long period of stability or very slow uplift, an initial abrupt increase in uplift rate allowed the isolation of the relict landscape, the development of the first knickpoint, and the intermediate segment in the stream longitudinal profiles (stage B of Figure 5). This event could have occurred between late Pliocene and the beginning of the Pleistocene, as lower Pleistocene alluvial and deltaic sediments that outcrop around the Sila document its erosion [Carobene and Damiani, 1985; Colella, 1988; Robustelli et al., 2009].

[42] A new increase in uplift rate generated the “second” knickpoint and the lower straight river profile segments (stage C in Figure 5). The rectilinear to convex profiles of these segments suggests the new uplift rate is not yet counterbalanced by erosion, maybe because the uplift is too recent and/or fast. Although a decrease in river incision rate could be attributed to climate change, this seems improbable as it would imply a persistent, long-term shift toward drier conditions, which have not been reported during the last million years. We made an attempt to set this uplift event in the Quaternary history of Sila by reconstructing the ancient

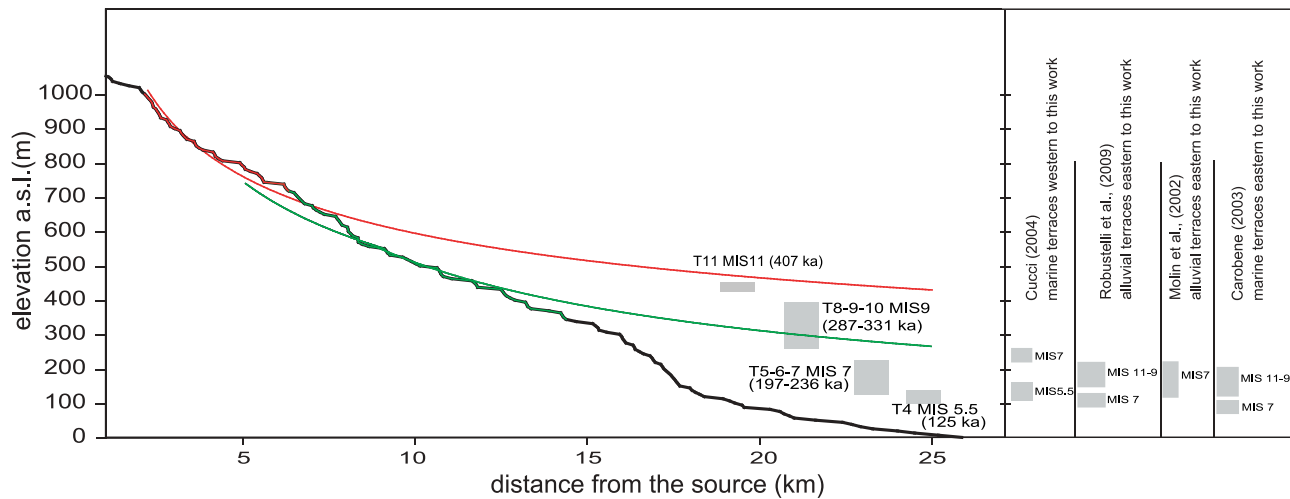


Figure 6. Relationship between modeled profiles of the intermediate segment of the Coriglianeto River and elevation of close marine terraces [Molin *et al.*, 2002; Carobene, 2003; Cucci, 2004; Ferranti *et al.*, 2009; Robustelli *et al.*, 2009]. Two portions of the intermediate segment have been modeled to provide upper and lower limit to segment projection. The elevation of alluvial and marine terraces located east and west of the Coriglianeto River valley are reported to the right.

longitudinal profile of the Coriglianeto River located in northern Sila, where several order of marine terraces have been reported and dated (Figure 6) [Molin *et al.*, 2002; Carobene, 2003; Cucci, 2004; Ferranti *et al.*, 2009; Robustelli *et al.*, 2009]. The knickpoint-bounded intermediate segment is a portion of the ancient river now perched by a renewal erosion wave propagating upstream from sea level and triggered by recent uplift. We reconstructed the entire ancient river profile before the abrupt increase in uplift rate by projecting the intermediate river segment downstream. To project the paleo-river we applied power law curve fitting of the actual intermediate segment following suggestion of Hoke *et al.* [2007]. The matching between dated marine terraces and the reconstructed ancient river profiles allowed us to suggest a possible age for the uplift event. Projection of the intermediate segment of Coriglianeto River matches the elevation between terrace T11 by Ferranti *et al.* [2009], which corresponds to MIS 11 (407 ka), and T9, which corresponds to MIS 9.3 (313 ka), indicating that an abrupt increase in uplift rate along the northern edge of the Sila massif occurred between 400 and 300 ka. Although the timing of the terrace orders appears very different, probably because of local tectonics and/or authors' interpretation (Figure 6), we argue for an abrupt increase in uplift rate occurred between 400 and 300 ka. This results in an uplift rate of 0.6–1 mm/yr, in agreement with the uplift rates calculated from terraces. This acceleration in the uplift rate around 400–300 ka agrees with previous models [Carobene, 2003; Bigazzi and Carobene, 2004; Robustelli *et al.*, 2009] and with recent OSL ages from the Bisignano Gilbert-fan delta in the Crati River valley, the most elevated fan delta terrace in the Sila region [Dewez *et al.*, 2008]. Alternatively, the marker for regional uplift could be assigned an early Pleistocene age (~700 ka), based on previous work that documented the transition from shelf-type to Gilbert-type to fan delta architecture [Colella, 1988] and fluvial

sediment deposited along the Coriglianeto river [Molin *et al.*, 2012] could be used as a marker for the regional uplift.

[43] The last phase of uplift increase was probably accompanied by fault activity which can be detected by the spatial distribution of steepness index. Rivers draining across active normal faults were perturbed by the fault slip that produced local convexities and increasing in steepness index. Corigliano-Rossano faults, Catanzaro fault, Eastern Crati fault and Piano Lago fault mark narrow belts of higher steepness indices (Figure 4b). Recent papers [Whittaker *et al.*, 2008; Cowie *et al.*, 2008] pointed out that significant changes in river profile shape are due by increasing in slip rate and not only by fault activity supporting for the Sila massif a coeval increasing of slip rate and regional uplift rate.

[44] Analysis of knickpoint elevations around the Sila massif further constrains the style of Sila massif uplift. Figure 7 shows the elevations of the two knickpoints around the Sila exhibit an undulatory pattern, reaching a minimum elevation along the northwestern flank of the Sila and a maximum elevation in the southeastern sector, supporting the uplift was not symmetric. Detachment-limited incision models predict that knickpoints propagate upstream following the same vertical velocity so that when knickpoints are generated by the same event they should have the same elevation [Whipple and Tucker, 1999; Niemann *et al.*, 2001]. As a consequence, this undulation may indicate that knickpoints underwent to differential uplift after their generation. In the northwestern corner of Sila a lower uplift rate could be related to the northward continuation of Cecita Lake fault, which downthrew the area [Molin *et al.*, 2012]. High uplift rates in the southeast are indicated by the morphology of the Crocchio River; its network is poorly developed, it is not deeply incised, its basin has a very elongated shape, and its longitudinal profile has a convex-up shape. These hydrographic features are consistent with a fluvial system in an early stage of development probably as a consequence of a recent strong uplift.

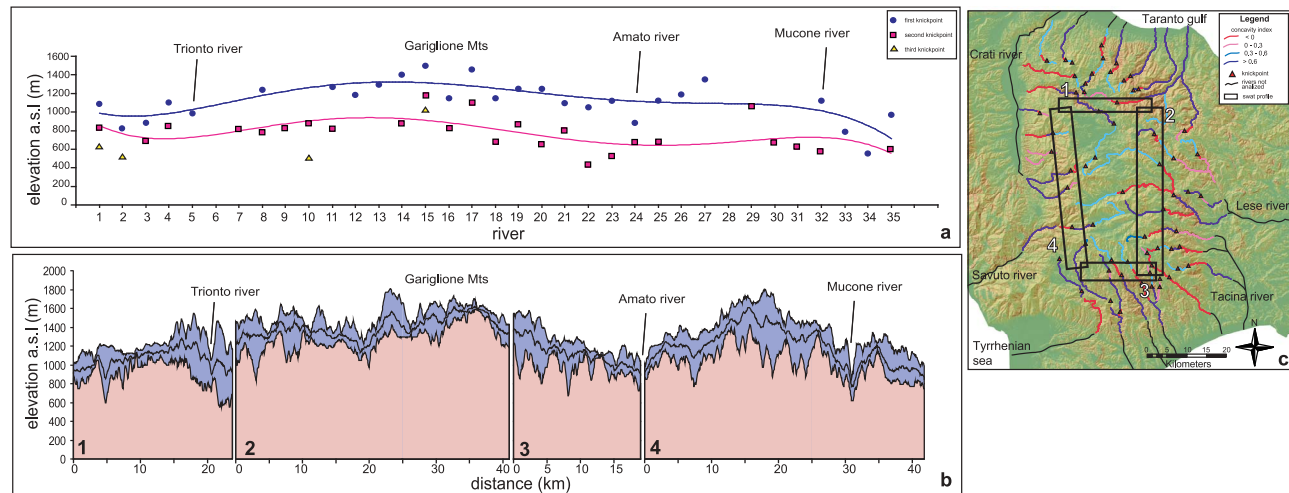


Figure 7. (a) Elevation of the knickpoints from each river analyzed (numbers as in Figure 3). Knickpoints have been separated into major knickpoints (blue circles), that mark the edge of the low-relief surface, intermediate knickpoints (purple squares), and rare minor knickpoints (yellow triangles). Elevations are plotted from the northwest (Coriglianeto River, n. 1) continuing clockwise around the massif. (b) Four swath profiles of elevation along the edge of the low-relief upland surface (see in the inset map), representing the pattern maximum, minimum and mean topography. Reference points are to match the elevation profiles with the knickpoints in Figure 7a. (c) Slope map of the Sila massif showing the trace of the swath profiles.

[45] In summary, in the case of the Sila Massif, a spatially uniform uplift alone is inadequate to account for the regional uplift signal preserved by geomorphic (or hydrographic) features. Instead, dome-style uplift, partially disturbed by local tectonics, is more appropriate. Indeed, many geological and morphological observations on Sila are consistent with this style of uplift, particularly (1) the tilting recorded by the Miocene to Pliocene sedimentary succession overlying the basement along the northern, eastern and southern flanks; (2) the presence of the old low-relief landscape not only atop Sila, but also on its flank interfluvies, as shown by geomorphology and cosmogenic analysis; (3) rectilinear to convex longitudinal profiles of the lowermost bedrock segments of rivers, although increased uplift rates could also be related to the onset of fault activity along structures bordering the Sila Massif [Colella, 1988; Robustelli *et al.*, 2009; Spina *et al.*, 2011; Faccenna *et al.*, 2011]; and (4) west to east asymmetric topography revealed by longitudinal river profiles.

6. Conclusions

[46] The Sila massif, along with the entire Calabrian Arc, underwent strong regional uplift constrained by well studied marine terraces. This uplift is likely related primarily to northwest-dipping subduction of the Ionian crust. For this reason the Sila Massif represents an ideal site where the study of landscape evolution may provide constraints on the uplift history of the Sila Massif and allows a reconstruction of the tectonic history of the region.

[47] The morphology of the Sila Massif is characterized by a high-standing low-relief landscape developed in nearly stable base level conditions. It contrasts with the fluvial valleys that deeply incise the massif flanks and represents, together with landsliding, the landscape response to a more recent uplift. In this morphological framework, we calculated hillslope erosion

rates by the content of the cosmogenic ^{10}Be in modern fluvial sand sampled in several sectors of the massif, and we carried out morphometric analysis on hydrography (river longitudinal profiles, and steepness and concavity indices). Our results are summarized as follows.

[48] (1) The lowest erosion rates (0.09 ± 0.01 to 0.13 ± 0.01 mm/yr) are located in the high-standing low-relief landscape while the highest values (up to 0.92 ± 0.08 mm/yr) are constrained (or ‘limited’) to the incised fluvial valleys on the massif flanks.

[49] (2) Most of the river longitudinal profiles are characterized by three segments separated by two major knickpoints. The highest reach, corresponding to the low-relief surface on top of Sila, is concave-up, smooth, and characterized by low values of normalized steepness index and concavity indices between 0.3 and 0.6. The “first” knickpoint corresponds to the boundary between the old upland landscape and the Sila flanks. The intermediate, shorter, stream profile segments show a variable shape, from a concave-up to straight, and sometimes convex-up. These intermediate stream segments are bounded at the downstream end by the “second” knickpoint. Downstream, the third stream reach has a nearly rectilinear profile, characterized by moderate steepness indices and concavity values between 0.14 and 2.2.

[50] Large variations in cosmogenic ^{10}Be erosion rates as well as disequilibrium river longitudinal profiles indicate a landscape in a transient state in response to a strong uplift not yet counterbalanced by erosion. More in detail, on the basis of the results we propose that: (1) the relict landscape, not yet reached by headward river incision, preserves the erosion rates of the pre-uplift stage; (2) the highest erosion rates (up to 0.92 ± 0.08 mm/yr) from small tributaries draining the massif flanks are representative of the current erosion processes acting on that part of the massif; (3) the intermediate

values of erosion rates are the result of sediment mixing between these two domains; (4) the downstream decrease in erosion rates that occurs in the Trionto and Lese rivers could testify to a component of sediment derived from slowly eroding relict landscape located on interfluvial Sila flanks that stand at lower altitude than the Sila top; (5) the “first” knickpoint indicates a sudden increase in uplift rate from stable base level conditions; (6) the “second” knickpoint is generated by a subsequent increase in uplift rate that occurred at 300–400 ka as indicated by marine terrace stratigraphy and paleo-longitudinal profile modeling; and (7) the regional uplift pattern of the Sila Massif is best explained as having a domal pattern that is locally disturbed by tectonic features.

[51] **Acknowledgments.** The authors would like to thank F. Pazzaglia for useful discussion and two anonymous reviewers for improvements to the manuscript. This work was supported in part by the National Science Foundation’s Continental Dynamics Program grant EAR-0208169, PRIME Lab at Purdue University, and the U.S. Geological Survey Mendenhall Postdoctoral Fellowship program (to A.J. Cyr).

References

- Ahnert, F. (1970), Functional relationship between denudation, relief, and uplift in large mid-latitude drainage basins, *Am. J. Sci.*, **268**, 243–263, doi:10.2475/ajs.268.3.243.
- Amato, A., and A. Cinque (1999), Erosional surfaces of the Campano-Lucano Apennines (S. Italy): Genesis, evolution, and tectonic implications, *Tectonophysics*, **315**, 251–267, doi:10.1016/S0040-1951(99)00288-7.
- Amodio-Morelli, L., et al. (1976), L’arco calabro-peloritano nell’orogene appennino-maghebide, *Mem. Soc. Geol. Ital.*, **17**, 1–60.
- Antonoli, F., L. Ferranti, K. Lambeck, S. Kershaw, V. Verrubbi, and G. Dai Pra (2006), Late Pleistocene to Holocene record of changing uplift rates in southern Calabria and northeastern Sicily (southern Italy, central Mediterranean Sea), *Tectonophysics*, **422**, 23–40, doi:10.1016/j.tecto.2006.05.003.
- Argentieri, A., M. Mattei, F. Rossetti, A. Argnani, F. Salvini, and R. Funicello (1998), Tectonic evolution of the Amantea Basin (Calabria, southern Italy): Comparing in-land and off-shore data, *Ann. Tecton.*, **12**, 79–96.
- Balescu, S., B. Dumas, P. Guermey, M. Lamothe, R. Lhenaff, and J. Raffy (1997), Thermoluminescence dating test of Pleistocene sediments from uplifted shorelines along the southwest coastline of the Calabrian peninsula (southern Italy), *Palaeogeogr. Palaeoclimatol. Palaeoecol.*, **130**, 25–41, doi:10.1016/S0031-0182(96)00119-8.
- Barrier, P., I. Di Geronimo, and G. Lanzafame (1986), I rapporti tra tettonica e sedimentazione nell’evoluzione recente dell’Aspromonte Occidentale (Calabria), *Riv. Ital. Paleontol. Stratigr.*, **91**(4), 537–556.
- Bigazzi, G., and L. Carobene (2004), Datazione di un livello cineritico del Pleistocene medio: Relazioni con sedimentazione, sollevamento e terrazzi marini nell’area Crosia-Calopezzati in Calabria (Italia), *Quaternario*, **17**, 151–163.
- Bigi, G., D. Cosentino, M. Parotto, R. Sartori, and P. Scandone (1990), Structural model of Italy, *Quad. Ric. Sci.*, **114**, 6 sheets, scale 1:500,000, C. N. R., Florence, Italy.
- Billi, A., D. Presti, C. Faccenna, G. Neri, and B. Orecchio (2007), Seismotectonics of the Nubia plate compressive margin in the south-Tyrrhenian region, Italy: Clues for subduction inception, *J. Geophys. Res.*, **112**, B08302, doi:10.1029/2006JB004837.
- Bonardi, G., P. De Capoa, A. Di Staso, V. Perrone, M. Sonnino, and M. Tramontana (2005), The age of the Paludi Formation: A major constraint to the beginning of the Apulia-verging orogenic transport in the northern sector of the Calabria-Peloritani Arc, *Terra Nova*, **17**, 331–337, doi:10.1111/j.1365-3121.2005.00618.x.
- Buiter, S. J. H., R. Govers, and M. J. R. Wortel (2002), Two-dimensional simulations of surface deformation caused by slab detachment, *Tectonophysics*, **354**, 195–210, doi:10.1016/S0040-1951(02)00336-0.
- Burbank, D. W. (2002), Rates of erosion and their implications for exhumation, *Mineral. Mag.*, **66**, 25–52, doi:10.1180/0026461026610014.
- Carobene, L. (2003), Genesi, età, sollevamento ed erosione dei terrazzi marini di Crosia-Calopezzati (Costa Ionica della Calabria– Italia), *Quaternario*, **16**(1), 43–90.
- Carobene, L., and A. V. Damiani (1985), Tettonica e sedimentazione pleistocenica nella media Valle del F. Crati (Calabria), *Boll. Soc. Geol. Ital.*, **104**, 93–114.
- Casero, P., and F. Roure (1994), Neogene Deformations at the Sicilian-North African Plate Boundary, in *Peri Tethyan Platforms*, edited by F. Roure, pp. 27–50, Ed. Technip, Paris.
- Cavazza, W., and P. G. DeCelles (1998), Upper Messinian siliciclastic rocks in southeastern Calabria (southern Italy): Paleotectonic and eustatic implications for the evolution of the central Mediterranean region, *Tectonophysics*, **298**, 223–241, doi:10.1016/S0040-1951(98)00186-3.
- Cello, G., I. Guerra, L. Tortorici, E. Turco, and R. Scarpa (1982), Geometry of the neotectonic stress field in southern Italy: Geological and seismological evidence, *J. Struct. Geol.*, **4**(4), 385–393, doi:10.1016/0191-8141(82)90030-X.
- Champagnac, J. D., P. Molnar, R. S. Anderson, C. Sue, and B. Delacou (2007), Quaternary erosion-induced isostatic rebound in the western Alps, *Geology*, **35**, 195–198, doi:10.1130/G23053A.1.
- Chiarabba, C., P. De Gori, and F. Speranza (2008), The southern Tyrrhenian subduction zone: Deep geometry, magmatism, and Plio-Pleistocene evolution, *Earth Planet. Sci. Lett.*, **268**, 408–423, doi:10.1016/j.epsl.2008.01.036.
- Ciaranfi, N., F. Ghisetti, M. Guida, G. Iaccarino, P. Pieri, L. Rapisardi, G. Ricchetti, M. Torre, L. Tortorici, and L. Vezzani (1983), Carta neotettonica dell’Italia meridionale, *Publ. 515*, 62 pp., C.N.R.–P.F.G., Bari, Italy.
- Cifelli, F., M. Mattei, and F. Rossetti (2007a), Tectonic evolution of arcuate mountain belts on top of a retreating subduction slab: The example of the Calabrian Arc, *J. Geophys. Res.*, **112**, B09101, doi:10.1029/2006JB004848.
- Cifelli, F., F. Rossetti, and M. Mattei (2007b), The architecture of brittle postorogenic extension: Results from an integrated structural and paleomagnetic study in north Calabria (southern Italy), *Geol. Soc. Am. Bull.*, **119**, 221–239, doi:10.1130/B25900.1.
- Colella, A. (1988), Fault-controlled marine Gilbert-type fan deltas, *Geology*, **16**, 1031–1034, doi:10.1130/0091-7613(1988)016<1031:FCMGTF>2.3.CO;2.
- Colella, A. (1995), Sedimentation, deformational events and eustasy in the perityrrhenian Amantea Basin: Preliminary synthesis, *G. Geol.*, **57**(1–2), 179–193.
- Colella, A., P. L. De Boer, and S. D. Nio (1987), Sedimentology of a marine intermontane Pleistocene Gilbert-type fan-delta complex in the Crati Basin, Calabria, southern Italy, *Sedimentology*, **34**, 721–736, doi:10.1111/j.1365-3091.1987.tb00798.x.
- Corbi, F., G. Fubelli, F. Luc, F. Muto, T. Pelle, G. Robustelli, F. Scarciglia, and F. Dramis (2009), Vertical movements in the Ionian margin of the Sila Massif (Calabria, Italy), *Ital. J. Geosci.*, **128**(3), 731–738, doi:10.3301/IJG.2009.128.3.731.
- Cosentino, D., and E. Gliozzi (1988), Considerazioni sulle velocità di sollevamento di depositi euriptenici dell’Italia Meridionale e della Sicilia, *Mem. Soc. Geol. Ital.*, **41**, 653–665.
- Cowie, P. A., A. C. Whittaker, M. Attal, G. Roberts, G. E. Tucker, and A. Ganas (2008), New constraints on sediment-flux-dependent river incision: Implications for extracting tectonic signals from river profiles, *Geology*, **36**(7), 535–538, doi:10.1130/G24681A.1.
- Critelli, S. (1990), Geological setting of the Trionto River basin, in *Symposium on Geomorphology of Active Tectonic Areas, Excursion Guidebook*, edited by M. Sorriso-Valvo, pp. 67–70, IGU-COMTAG, Cosenza, Italy.
- Critelli, S., and E. Le Pera (1998), Post-Oligocene sediment-dispersal systems and unroofing history of the Calabrian microplate, Italy, *Int. Geol. Rev.*, **40**(7), 609–637, doi:10.1080/00206819809465227.
- Cucci, L. (2004), Raised marine terraces in the Northern Calabrian Arc (Southern Italy): A ~600 Kyr-long geological record of regional uplift, *Ann. Geophys.*, **47**, 1391–1406.
- Cucci, L., and R. Cinti (1998), Regional uplift and local tectonic deformation recorded by the Quaternary marine terraces on the Ionian coast of northern Calabria, *Tectonophysics*, **292**, 67–83, doi:10.1016/S0040-1951(98)00061-4.
- D’Agostino, N., and G. Selvaggi (2004), Crustal motion along the Eurasia–Nubia plate boundary in the Calabrian Arc and Sicily and active extension in the Messina Straits from GPS measurements, *J. Geophys. Res.*, **109**, B11402, doi:10.1029/2004JB002998.
- Dewez, T., C. Stark, L. Seeberg, S. Huot, M. Lamothe, M. Cardinali, and F. Guzzetti (2008), Late Quaternary uplift and coastal landscape evolution in northern Calabria, *Eos Trans. AGU*, **89**(53), Fall Meet. Suppl., Abstract T53B-1930.
- Dietrich, D. (1976), La geologia della Catena Costiera Calabria tra Cetraro e Guardia Piemontese, *Mem. Soc. Geol. Ital.*, **17**, 61–121.
- Dietrich, W. E., D. G. Bellugi, L. S. Sklar, J. D. Stock, A. M. Heimsath, and J. J. Roering (2003), Geomorphic Transport Laws for Predicting Landscape Form and Dynamics, in *Prediction in Geomorphology*, *Geophys. Monogr. Ser.*, vol. 135, edited by P. W. Wilcock and R. M. Iverson, pp. 103–132, AGU, Washington, D. C., doi:10.1029/135GM09.

- Doglioni, C., E. Carminati, M. Cuffaro, and D. Scrocca (2007), Subduction kinematics and dynamic constraints, *Earth Sci. Rev.*, 83, 125–175, doi:10.1016/j.earscirev.2007.04.001.
- Dramis, F. (1992), Il ruolo dei sollevamenti tettonici a largo raggio nella genesi del rilievo appenninico, *Stud. Geol. Camerti, Vol. Spec.*, 1, 9–15.
- Dramis, F., B. Gentili, and G. Pambianchi (1990), Geomorphological scheme of the River Trionto basin, in *Symposium on Geomorphology of Active Tectonic Areas, Excursion Guidebook*, edited by M. Sorriso-Valvo, pp. 63–66, IGU-COMTAG, Cosenza, Italy.
- Dumas, B., P. Gueremy, R. Lhenaff, and J. Raffy, (1987), Rates of uplift as shown by raised Quaternary shorelines in Southern Calabria (Italy), *Z. Geomorphol., Suppl.*, 63, 119–132.
- Faccenna, C., C. Piromallo, A. Crespo-Blanc, L. Jolivet, and F. Rossetti (2004), Lateral slab deformation and the origin of the Western Mediterranean arcs, *Tectonics*, 23, TC1012, doi:10.1029/2002TC001488.
- Faccenna, C., L. Civetta, M. D'Antonio, F. Funiello, L. Margheriti, and C. Piromallo (2005), Constraints on mantle circulation around the deforming Calabrian slab, *Geophys. Res. Lett.*, 32, L06311, doi:10.1029/2004GL021874.
- Faccenna, C., P. Molin, B. Orecchio, V. Olivetti, O. Bellier, F. Funiello, L. Minelli, C. Piromallo, and A. Billi (2011), Topography of the Calabria subduction zone (southern Italy): Clues for the origin of Mt. Etna, *Tectonics*, 30, TC1003, doi:10.1029/2010TC002694.
- Ferranti, L., et al. (2006), Markers of the last interglacial sea level high stand along the coast of Italy: Tectonic implications, *Quat. Int.*, 145–146, 30–54, doi:10.1016/j.quaint.2005.07.009.
- Ferranti, L., E. Santoro, M. E. Mazzella, C. Monaco, and D. Morelli (2009), Active transpression in the northern Calabria Apennines, southern Italy, *Tectonophysics*, 476, 226–251, doi:10.1016/j.tecto.2008.11.010.
- Flint, J. J. (1974), Stream gradient as a function of order, magnitude, and discharge, *Water Resour. Res.*, 10, 969–973, doi:10.1029/WR010i005p0969.
- Galli, P., and V. Bosi (2003), Catastrophic 1638 earthquakes in Calabria (southern Italy): New insights from paleoseismological investigation, *J. Geophys. Res.*, 108(B1), 2004, doi:10.1029/2001JB001713.
- Galli, P., and V. Scionti (2006), Two unknown M > 6 historical earthquakes revealed by paleoseismological and archival researches in eastern Calabria (southern Italy). Seismotectonic implication, *Terra Nova*, 18, 44–49, doi:10.1111/j.1365-3121.2005.00658.x.
- Ghisetti, F. (1981), Upper Pliocene-Pleistocene uplift rates as indicators of neotectonic pattern, *Z. Geomorphol.*, 40, 93–118.
- Ghisetti, F., and L. Vezzani (1982), Different styles of deformation in the Calabrian arc (southern Italy): Implications for a seismotectonic zoning, *Tectonophysics*, 85, 149–165, doi:10.1016/0040-1951(82)90101-9.
- Giardini, D., and M. Velsonà (1991), Deep seismicity of the Tyrrhenian Sea, *Terra Nova*, 3, 57–64, doi:10.1111/j.1365-3121.1991.tb00844.x.
- Giunchi, C., R. Sabadini, E. Boschi, and P. Gasperini (1996), Dynamic models of subduction: Geophysical and geological evidence in the Tyrrhenian Sea, *Geophys. J. Int.*, 126, 555–578, doi:10.1111/j.1365-246X.1996.tb05310.x.
- Gliozzi, E. (1987), I terrazzi del Pleistocene superiore della penisola di Crotona (Calabria), *Geol. Rom.*, 26, 17–79.
- Goes, S., D. Giardini, S. Jenny, C. Hollenstein, H. G. Kahle, and A. Geiger (2004), A recent tectonic reorganization in the south-central Mediterranean, *Earth Planet. Sci. Lett.*, 226, 335–345, doi:10.1016/j.epsl.2004.07.038.
- Granger, D. E., and A. L. Smith (2000), Dating buried sediments using radioactive decay and muogenic production of ²⁶Al and ¹⁰Be, *Nucl. Instrum. Methods Phys. Res., Sect. B*, 172, 822–826, doi:10.1016/S0168-583X(00)00087-2.
- Granger, D. E., C. S. Riebe, J. W. Kirchner, and R. Finkel (2001), Modulation of erosion on steep granitic slopes by boulder armoring, as revealed by cosmogenic ²⁶Al and ¹⁰Be, *Earth Planet. Sci. Lett.*, 186, 269–281, doi:10.1016/S0012-821X(01)00236-9.
- Guérémy, P. (1972), La Calabre centrale et septentrionale. Guide d'excursion géomorphologique, *Trav. Inst. Geogr. Reims*, 10, 1–128.
- Gvirtzman, Z., and A. Nur (1999), The formation of Mount Etna as the consequence of slab rollback, *Nature*, 401, 782–785, doi:10.1038/44555.
- Hack, J. T. (1957), Studies of longitudinal profiles in Virginia and Maryland, *U.S. Geol. Surv. Prof. Pap.*, 294-B, 45–97.
- Hack, J. T. (1960), Interpretation of erosional topography in humid temperature regions, *Am. J. Sci.*, 258-A, 80–97.
- Hancock, G. S., R. S. Anderson, and K. X. Whipple (1998), Beyond power: Bedrock river incision process and form, in *Rivers Over Rock: Fluvial Processes in Bedrock Channels*, *Geophys. Monogr. Ser.*, vol. 107, edited by J. Tinkler and E. Wohl, pp. 35–60, AGU, Washington, D. C., doi:10.1029/GM107p0035.
- Henderson, G. (1970), Carta Geologica della Calabria, 183 sheets, scale 1:25000, La Cassa del Mezzogiorno, Rome.
- Hoke, G. D., B. L. Isacks, T. E. Jordan, N. Blanco, A. J. Tomlinson, and J. Ramezani (2007), Geomorphic evidence for post-10 Ma uplift of the western flank of the central Andes 18°30'–22°S, *Tectonics*, 26, TC5021, doi:10.1029/2006TC002082.
- Howard, A. D., W. E. Dietrich, and M. A. Seidl (1994), Modeling fluvial erosion on regional to continental scales, *J. Geophys. Res.*, 99, 13,971–13,986, doi:10.1029/94JB00744.
- Kastens, K. A., J. Mascle, and O. L. S. Party (1988), ODP Leg 107 in the Tyrrhenian Sea: Insights into passive margin and backarc basin evolution, *Geol. Soc. Am. Bull.*, 100, 1140–1156, doi:10.1130/0016-7606(1988)100<1140:OLITTS>2.3.CO;2.
- Kirby, E., and K. X. Whipple (2001), Quantifying differential rock-uplift rates via stream profile analysis, *Geology*, 29, 415–418, doi:10.1130/0091-7613(2001)029<0415:QDRURV>2.0.CO;2.
- Kirby, E., K. X. Whipple, W. Tang, and Z. Chen (2003), Distribution of active rock uplift along the eastern margin of the Tibetan Plateau: Inferences from bedrock channel longitudinal long profiles, *J. Geophys. Res.*, 108(B4), 2217, doi:10.1029/2001JB000861.
- Knott, S. D., and E. Turco (1991), Late Cenozoic kinematics of the Calabrian arc, southern Italy, *Tectonics*, 10, 1164–1172, doi:10.1029/91TC01535.
- Kobor, J. S., and J. J. Roering (2004), Systematic variation of bedrock channel gradients in the central Oregon Coast Range: Implications for rock uplift and shallow landsliding, *Geomorphology*, 62, 239–256, doi:10.1016/j.geomorph.2004.02.013.
- Lague, D., P. Davy, and A. Crave (2000), Estimating uplift rate and erodibility from the area-slope relationship: Examples from Brittany (France) and numerical modelling, *Phys. Chem. Earth, Part A*, 25(6–7), 543–548.
- Lal, D. (1991), Cosmic ray labeling of erosion surfaces: In situ nuclide production rates and erosion models, *Earth Planet. Sci. Lett.*, 104, 424–439, doi:10.1016/0012-821X(91)90220-C.
- Lanzafame, G., and L. Tortorici (1981), La tettonica recente della Valle del Fiume Crati (Calabria), *Geogr. Fis. Din. Quat.*, 4, 11–21.
- Lanzafame, G., P. Spadea, and L. Tortorici (1979), Mesozoic ophiolites of the northern Calabria and Lucanian Apennine (southern Italy), *Ophioliti*, 4(2), 173–182.
- Leopold, L. B., G. Wolman, and J. B. Miller (1964), *Fluvial Processes in Geomorphology*, 522 pp., W. H. Freeman, San Francisco, Calif.
- Le Pera, E., and M. Sorriso-Valvo (2000), Weathering and morphogenesis in a Mediterranean climate, Calabria, Italy, *Geomorphology*, 34, 251–270, doi:10.1016/S0169-555X(00)00012-X.
- Mackin, J. H. (1948), Concept of the graded river, *Geol. Soc. Am. Bull.*, 59, 463–512, doi:10.1130/0016-7606(1948)59[463:COTGR]2.0.CO;2.
- Malinverno, A., and W. Ryan (1986), Extension in the Tyrrhenian sea and shortening in the Apennines as result of arc migration driven by sinking of the lithosphere, *Tectonics*, 5, 227–245, doi:10.1029/TC005i002p00227.
- Masarik, J., and R. C. Reedy (1995), Terrestrial cosmogenic-nuclide production systematics calculated from numerical simulations, *Earth Planet. Sci. Lett.*, 136, 381–395, doi:10.1016/0012-821X(95)00169-D.
- Matano, F., and S. Di Nocera (1999), Weathering patterns in the Sila Massif (Northern Calabria Italy), *Quaternario*, 12, 141–148.
- Mattei, M., F. Cifelli, and N. D'Agostino (2007), The evolution of the Calabrian Arc: Evidence from paleomagnetic and GPS observations, *Earth Planet. Sci. Lett.*, 263, 259–274, doi:10.1016/j.epsl.2007.08.034.
- Miyauchi, T., G. Dai Pra, and S. Sylos Labini (1994), Geochronology of Pleistocene marine terraces and regional tectonics in the Tyrrhenian coast of South Calabria, Italy, *Quaternario*, 7, 17–34.
- Molin, P., F. Dramis and E. Lupia Palmieri (2002), The Plio-Quaternary uplift of the Ionian northern Calabria coastal belt between Corigliano Calabro e Capo Trionto, *Stud. Geol. Camerti*, 2002, 135–145.
- Molin, P., F. J. Pazzaglia, and F. Dramis (2004), Geomorphic expression of active tectonics in a rapidly deforming forearc, Sila Massif, Calabria, southern Italy, *Am. J. Sci.*, 304, 559–589, doi:10.2475/ajs.304.7.559.
- Molin, P., G. Fubelli, and F. Dramis (2012), The tectonic influence on drainage evolution in an uplifting area: The case of the Sila Greca (Calabria, Italy), *Geogr. Fis. Din. Quat.*, in press.
- Molnar, P., and P. England (1990), Late Cenozoic uplift of mountain ranges and global climate change: Chicken or egg?, *Nature*, 346, 29–34, doi:10.1038/346029a0.
- Monaco, C., and L. Tortorici (2000), Active faulting in the Calabrian arc and eastern Sicily, *J. Geodyn.*, 29, 407–424, doi:10.1016/S0264-3707(99)00052-6.
- Montgomery, D. R., and E. Foufoula-Georgiou (1993), Channel network source representation using digital elevation models, *Water Resour. Res.*, 29, 3925–3934, doi:10.1029/93WR02463.
- Moretti, A. (2000), Il database delle faglie capaci della Calabria: Stato attuale delle conoscenze, in *Le Ricerche del GNDT nel Campo della Pericolosità Sismica (1996–1999)*, edited by F. Galadini, C. Meletti, and A. Rebez, pp. 219–226, C. N. R., Rome.

- Moretti, A., and I. Guerra (1997), Tettonica dal Messiniano ad oggi in Calabria: Implicazioni sulla geodinamica del sistema Tirreno-Arco calabro, *Boll. Soc. Geol. Ital.*, *116*, 125–142.
- Nicolosi, J., F. Speranza, and M. Chiappini (2006), Ultrafast oceanic spreading of the Marsili Basin, southern Tyrrhenian Sea: Evidence from magnetic anomaly analysis, *Geology*, *34*, 717–720, doi:10.1130/G22555.1.
- Niemann, J. D., N. M. Gasparini, G. E. Tucker, and R. L. Bras (2001), A quantitative evaluation of Playfair's Law and its use in testing long-term stream erosion models, *Earth Surf. Processes Landforms*, *26*, 1317–1332, doi:10.1002/esp.272.
- Niemi, N. A., O. Oskin, D. W. Burbank, A. M. Heimsath, and E. J. Gabel (2005), Effects of bedrock landslides on cosmogenically determined erosion rates, *Earth Planet. Sci. Lett.*, *237*, 480–498, doi:10.1016/j.epsl.2005.07.009.
- Nishiizumi, K., M. Imamura, M. W. Caffee, J. R. Southon, R. C. Finkel, and J. McAninch (2007), Absolute calibration of ¹⁰Be AMS standards, *Nucl. Instrum. Methods Phys. Res., Sect. B*, *258*(2), 403–413.
- Ogniben, L. (1973), Schema geologico della Calabria in base ai dati odierni, *Geol. Rom.*, *12*, 243–585.
- Ortolani, F., M. Torre, and S. Di Nocera (1979), I depositi altomiocenici del bacino di Amantea (Catena Costiera calabro), *Boll. Soc. Geol. Ital.*, *98*, 559–587.
- Palmentola, G., L. Carobene, G. Mastronuzzi, and P. Sansò (1990), I terrazzi marini Pleistocenici della Penisola di Crotona (Calabria), *Geogr. Fis. Din. Quat.*, *13*, 75–80.
- Patacca, E., R. Sartori, and P. Scandone (1990), Tyrrhenian basin and Apenninic arcs. Kinematic relations since late Tortonian times, *Mem. Soc. Geol. Ital.*, *45*, 425–451.
- Pazzaglia, F. J., T. W. Gardner, and D. J. Merritts (1998), Bedrock fluvial incision and longitudinal profile development over geologic time scales determined by fluvial terraces, in *Rivers Over Rock: Fluvial Processes in Bedrock Channels*, *Geophys. Monogr. Ser.*, vol. 107, edited by J. Tinkler and E. Wohl, pp. 207–235, AGU, Washington, D. C., doi:10.1029/GM107p0207.
- Piana Agostinetti, N., and A. Amato (2009), Moho depth and Vp/Vs ratio in peninsular Italy from teleseismic receiver functions, *J. Geophys. Res.*, *114*, B06303, doi:10.1029/2008JB005899.
- Pirazzoli, P. A., G. Mastronuzzi, J. F. Saliège, and P. Sansò (1997), Late Holocene emergence in Calabria, Italy, *Mar. Geol.*, *141*, 61–70, doi:10.1016/S0025-3227(97)00057-1.
- Robustelli, G., F. Lucà, F. Corbi, T. Pelle, F. Dramis, G. Fubelli, F. Scarciglia, F. Muto, and D. Cugliari (2009), Alluvial terraces on the Ionian coast of northern Calabria, southern Italy: Implications for tectonic and sea level controls, *Geomorphology*, *106*, 165–179, doi:10.1016/j.geomorph.2008.12.010.
- Romeo, M., and L. Tortorici (1980), Stratigrafia dei depositi miocenici della Catena Costiera calabro meridionale e della media Valle del F. Crati (Calabria), *Boll. Soc. Geol. Ital.*, *99*, 303–318.
- Rosenbaum, G., and G. S. Lister (2004), Neogene and Quaternary rollback evolution of the Tyrrhenian Sea, the Apennines, and the Sicilian Maghrebides, *Tectonics*, *23*, TC1013, doi:10.1029/2003TC001518.
- Rossetti, F., C. Faccenna, B. Goffé, P. Monié, A. Argentieri, R. Funicello, and M. Mattei (2001), Alpine structural and metamorphic signature of the Sila Piccola Massif nappe stack (Calabria, Italy): Insights for the tectonic evolution of the Calabrian Arc, *Tectonics*, *20*, 112–133, doi:10.1029/2000TC900027.
- Royden, L. H. (1993), Evolution of retreating subduction boundaries formed during continental collision, *Tectonics*, *12*, 629–638, doi:10.1029/92TC02641.
- Sarti, M. (2010), San Giovanni in Fiore, in *Carta Geologica d'Italia*, foglio 561, scale 1:50000, ISPRA–Serv. Geol., Rome.
- Sartori, R., and ODP Leg 107 Scientific Staff (1989), Drillings of ODP Leg 107 in the Tyrrhenian Sea: Tentative basin evolution compared to deformations in the surrounding chains, in *The Lithosphere in Italy: Advances in Earth Science Research*, edited by A. Boriani et al., pp. 139–156, Accad. Naz. Lincei, Rome.
- Scarciglia, F., E. Le Pera, G. Vecchio, and S. Critelli (2005), The interplay of geomorphic processes and soil development in an upland environment, Calabria, South Italy, *Geomorphology*, *69*, 169–190, doi:10.1016/j.geomorph.2005.01.003.
- Schaller, M., and T. A. Ehlers (2006), Limits to quantifying climate driven changes in denudation rates with cosmogenic radionuclides, *Earth Planet. Sci. Lett.*, *248*, 153–167, doi:10.1016/j.epsl.2006.05.027.
- Schaller, M., F. von Blanckenburg, A. Veldkamp, L. A. Tebbens, N. Hovius, and P. W. Kubik (2002), A 30,000 yr record of erosion rates from cosmogenic ¹⁰Be in Middle European river terraces, *Earth Planet. Sci. Lett.*, *204*, 307–320, doi:10.1016/S0012-821X(02)00951-2.
- Schoenbohm, L. M., K. X. Whipple, B. C. Burchfiel, and L. Chen (2004), Geomorphic constraints on surface uplift, exhumation, and plateau growth in the Red River region, Yunnan Province, China, *Geol. Soc. Am. Bull.*, *116*, 895–909, doi:10.1130/B25364.1.
- Schorghofer, N., and D. H. Rothman (2002), A causal relations between topographic slope and drainage area, *Geophys. Res. Lett.*, *29*(13), 1633, doi:10.1029/2002GL015144.
- Schumm, S. A., and R. W. Lichty (1965), Time, space, and causality in geomorphology, *Am. J. Sci.*, *263*, 110–119, doi:10.2475/ajs.263.2.110.
- Selvaggi, G., and C. Chiarabba (1995), Seismicity and P wave velocity image of the Southern Tyrrhenian subduction zone, *Geophys. J. Int.*, *121*, 818–826, doi:10.1111/j.1365-246X.1995.tb06441.x.
- Sklar, L., and W. E. Dietrich (1998), River longitudinal profiles and bedrock incision models: Stream power and the influence of sediment supply, in *Rivers Over Rock: Fluvial Processes in Bedrock Channels*, *Geophys. Monogr. Ser.*, vol. 107, edited by J. Tinkler and E. Wohl, pp. 237–260, AGU, Washington, D. C., doi:10.1029/GM107p0237.
- Snyder, N. P., K. X. Whipple, G. E. Tucker, and D. J. Merritts (2000), Landscape response to tectonic forcing: Digital elevation model analysis of stream profiles in the Mendocino triple junction region, Northern California, *Geol. Soc. Am. Bull.*, *112*, 1250–1263, doi:10.1130/0016-7606(2000)112<1250:LRTTFD>2.0.CO;2.
- Sorriso-Valvo, M. (1993), The geomorphology of Calabria - A sketch, *Geogr. Fis. Din. Quat.*, *16*, 75–80.
- Sorriso-Valvo, M., and A. G. Sylvester (1993), The relationship between geology and landforms along a coastal mountain front, northern Calabria, Italy, *Earth Surf. Processes Landforms*, *18*, 257–273, doi:10.1002/esp.3290180307.
- Speranza, F., M. Mattei, L. Sagnotti, and F. Grasso (2000), Rotational differences between the northern and southern Tyrrhenian domains: Paleomagnetic constraints from the Amantea basin (Calabria, Italy), *J. Geol. Soc.*, *157*, 327–334, doi:10.1144/jgs.157.2.327.
- Spina, V., P. Galli, E. Tondi, S. Critelli, and G. Cello (2007), Kinematics and structural properties of an active fault zone in the Sila Massif (Northern Calabria, Italy), *Boll. Soc. Geol. Ital.*, *126*, 2.
- Spina, V., E. Tondi, and S. Mazzoli (2011), Complex basin development in a wrench-dominated back-arc area: Tectonic evolution of the Crati Basin, Calabria, Italy, *J. Geodyn.*, *51*, 90–109, doi:10.1016/j.jog.2010.05.003.
- Stirling, C. H., T. M. Esat, M. T. McCulloch, and K. Lambeck (1995), High-precision U-series dating of corals from Western Australia and implications for the timing and duration of the Last Interglacial, *Earth Planet. Sci. Lett.*, *135*, 115–130, doi:10.1016/0012-821X(95)00152-3.
- Stock, G. M., K. L. Frankel, T. A. Ehlers, M. Schaller, S. M. Briggs, and R. C. Finkel (2009), Spatial and temporal variations in denudation of the Wasatch Mountains, Utah, USA, *Lithosphere*, *1*, 34–40, doi:10.1130/L15.1.
- Stock, J. D., and D. R. Montgomery (1999), Geologic constraints on bedrock incision using the stream power law, *J. Geophys. Res.*, *104*, 4983–4993, doi:10.1029/98JB02139.
- Stone, J. O. (2000), Air pressure and cosmogenic isotope production, *J. Geophys. Res.*, *105*, 23,753–23,759, doi:10.1029/2000JB900181.
- Suhadolc, P., and G. F. Panza (1989), Physical properties of the lithosphere-asthenosphere system in Europe from geophysical data, in *The Lithosphere in Italy: Advances in Earth Science Research*, edited by A. Boriani et al., pp. 15–37, Accad. Naz. Lincei, Rome.
- Tansi, C., F. Muto, S. Critelli, and G. Iovine (2007), Neogene–Quaternary strike-slip tectonics in the central Calabrian Arc (southern Italy), *J. Geodyn.*, *43*, 393–414, doi:10.1016/j.jog.2006.10.006.
- Thomson, S. N. (1994), Fission track analysis of the crystalline basement rocks of the Oligo-Miocene late-orogenic extension and erosion, *Tectonophysics*, *238*, 331–352, doi:10.1016/0040-1951(94)90063-9.
- Thomson, S. N. (1998), Assessing the nature of tectonic contact using fission track thermochronology: An example from the Calabrian Arc, southern Italy, *Terra Nova*, *10*, 32–36, doi:10.1046/j.1365-3121.1998.00165.x.
- Tortorici, G., M. Bianca, G. de Guidi, C. Monaco, and L. Tortorici (2003), Fault activity and marine terracing in the Capo Vaticano area (southern Calabria) during the Middle-Late Quaternary, *Quat. Int.*, *101–102*, 269–278, doi:10.1016/S1040-6182(02)00107-6.
- Tortorici, L. (1981), Analisi delle deformazioni fragili dei sedimenti postorogeni della Calabria settentrionale, *Boll. Soc. Geol. Ital.*, *100*, 291–308.
- Tortorici, L., C. Monaco, C. Tansi, and O. Cocina (1995), Recent and active tectonics in the Calabrian Arc (southern Italy), *Tectonophysics*, *243*, 37–55, doi:10.1016/0040-1951(94)00190-K.
- Van Dijk, J. P., et al. (2000), A regional structural model for the northern sector of the Calabrian Arc (southern Italy), *Tectonophysics*, *324*, 267–320, doi:10.1016/S0040-1951(00)00139-6.
- Vezzani, L. (1968), I terreni plio-pleistocenici del basso Crati (Cosenza), *Atti Accad. Gioenia Sci. Nat. Catania*, *20*, 28–84.
- von Blanckenburg, F. (2005), The control mechanisms of erosion and weathering at basin scale from cosmogenic nuclides in river sediment, *Earth Planet. Sci. Lett.*, *237*, 462–479, doi:10.1016/j.epsl.2005.06.030.

- Westaway, R. (1993), Quaternary uplift of southern Italy, *J. Geophys. Res.*, 98(B12), 21,741–21,772, doi:10.1029/93JB01566.
- Whipple, K. X. (2001), Fluvial landscape response time: how plausible is steady state denudation?, *Am. J. Sci.*, 301, 313–325, doi:10.2475/ajs.301.4-5.313.
- Whipple, K. X. (2004), Bedrock rivers and the geomorphology of active orogen, *Annu. Rev. Earth Planet. Sci.*, 32, 151–185, doi:10.1146/annurev.earth.32.101802.120356.
- Whipple, K. X., and G. E. Tucker (1999), Dynamics of the stream power river incision model: Implications for height limits of mountain ranges, landscape response times scales, and research needs, *J. Geophys. Res.*, 104, 17,661–17,674, doi:10.1029/1999JB900120.
- Whittaker, A. C., M. Attal, P. A. Cowie, G. E. Tucker, and G. Roberts (2008), Decoding temporal and spatial patterns of fault uplift using transient river long profiles, *Geomorphology*, 100, 506–526, doi:10.1016/j.geomorph.2008.01.018.
- Willett, S. D., and M. T. Brandon (2002), On steady states in mountain belts, *Geology*, 30, 175–178, doi:10.1130/0091-7613(2002)030<0175:OSSIMB>2.0.CO;2.
- Wittmann, H., F. von Blanckenburg, T. Kruesmann, K. P. Norton, and P. W. Kubik (2007), Relation between rock uplift and denudation from cosmogenic nuclides in river sediment in the Central Alps of Switzerland, *J. Geophys. Res.*, 112, F04010, doi:10.1029/2006JF000729.
- Wobus, C., K. X. Whipple, E. Kirby, N. P. Snyder, J. Johnson, K. Spyropolou, B. T. Crosby, and D. Sheehan (2006), Tectonics from topography: Procedures, promise, and pitfalls, in *Tectonics, Climate, and Landscape Evolution*, edited by S. D. Willett et al., *Spec. Pap. Geol. Soc. Am.*, 398, 55–74.
- Wortel, M. J. R., and W. Spakman (2000), Subduction and slab detachment in the Mediterranean-Carpathian region, *Science*, 290, 1910–1917, doi:10.1126/science.290.5498.1910.
- Yanites, B. J., G. E. Tucker, and R. S. Anderson (2009), Numerical and analytical models of cosmogenic radionuclide dynamics in landslide-dominated drainage basins, *J. Geophys. Res.*, 114, F01007, doi:10.1029/2008JF001088.
- Zecchin, M., R. Nalinc, and C. Rodad (2004), Raised Pleistocene marine terraces of the Crotona peninsula (Calabria, southern Italy): Facies analysis and organization of their deposits, *Sediment. Geol.*, 172, 165–185, doi:10.1016/j.sedgeo.2004.08.003.